Naval Research Laboratory

Stennis Space Center, MS 39529-5004

Bathymetry from Hyperspectral Sensors: A Preliminary Analysis of the Problem

RONALD J. HOLYER
JUANITA C. SANDIDGE

Remote Sensing Applications Branch
Oceanography Division

May 20, 1999

19990628 012

DTIC QUALITY INSPECTED 4

REPORT DOCUMENTATION PAGE

1. AGENCY USE ONLY *(Leave blank)*	2. REPORT DATE May 20, 1999	3. REPORT TYPE AND DATES COVERED Final

4. TITLE AND SUBTITLE

Bathymetry from Hyperspectral Sensors: A Preliminary Analysis of the Problem

6. AUTHOR(S)

Ronald J. Holyer and Juanita C. Sandidge

5. FUNDING NUMBERS

Job Order No.

Program Element No. 0605013N

Project No. F1947

Task No.

Accession No.

7. PERFORMING ORGANIZATION NAME(S) AND ADDRESS(ES)

Naval Research Laboratory
Oceanography Division
Stennis Space Center, MS 39529-5004

8. PERFORMING ORGANIZATION REPORT NUMBER

NRL/FR/7341--98-9690

9. SPONSORING/MONITORING AGENCY NAME(S) AND ADDRESS(ES)

Navy Office for the Tactical Exploitation of National Capabilities
2511 South Jefferson Davis Highway
Arlington, VA 22202

10. SPONSORING/MONITORING AGENCY REPORT NUMBER

11. SUPPLEMENTARY NOTES

12a. DISTRIBUTION/AVAILABILITY STATEMENT

Approved for public release; distribution unlimited.

12b. DISTRIBUTION CODE

13. ABSTRACT *(Maximum 200 words)*

Water depth, bottom reflectance, inherent optical properties of the water column (scattering, absorption, and fluorescence), and illumination conditions combine to determine the upwelling spectral radiance of coastal waters. If these complex optical relationships could be quantified, it would be possible to extract coastal information from spectral radiance data. We use data from the Airborne Visible/Infrared Imaging Spectrometer (AVIRIS) to begin to characterize these relationships as a first step toward development of algorithms for retrieval of water depth from hyperspectral imagery. Data are analyzed for two areas: the western coast of Florida in the Tampa Bay area and the Florida Keys between Upper Matecumbe and Plantation Keys. A neural network approach has been used to demonstrate retrieval of reasonable depths from spectral radiance over a depth range of 0 to 6 m. The ability of the neural network to generalize, producing algorithms with some degree of universality among diverse coastal environments, has been investigated in a preliminary fashion.

14. SUBJECT TERMS

oceanography, bathymetry, hyperspectral imagery, spectral radiance

15. NUMBER OF PAGES
34

16. PRICE CODE

17. SECURITY CLASSIFICATION OF REPORT	18. SECURITY CLASSIFICATION OF THIS PAGE	19. SECURITY CLASSIFICATION OF ABSTRACT	20. LIMITATION OF ABSTRACT
Unclassified	Unclassified	Unclassified	Same as Report

CONTENTS

EXECUTIVE SUMMARY

Water depth, bottom reflectance, inherent optical properties of the water column (scattering, absorption, and fluorescence), and illumination conditions combine to determine the upwelling spectral radiance of coastal waters. If these complex optical relationships could be quantified, it would be possible to extract coastal information from spectral radiance data. We use data from the Airborne Visible/Infrared Imaging Spectrometer to begin to characterize these relationships as a first step toward development of algorithms for retrieval of one of these parameters, water depth, from hyperspectral imagery. Data are analyzed for two areas: the western coast of Florida in the Tampa Bay area and the Florida Keys between Upper Matecumbe and Plantation Keys. Issues related to the number of spectral bands required for depth retrieval and the optimal wavelengths of these bands are investigated. The sensitivity of retrieved depth values to instrument signal-to-noise ratio and sensor calibration error is presented. The neural network approach has been used to demonstrate retrieval of reasonable depths from spectral radiance over a depth range of 0 to 6 m. Retrieved depths for Tampa Bay are accurate to a root mean squared (RMS) error of 0.84 m relative to depths in the National Ocean Survey Hydrographic Data Base, and the Keys retrievals have an RMS error of 0.39 m relative to a bathymetric survey conducted to support this study. A neural network trained on a combination of the two data sets results in a combined RMS error of 0.48 m, nearly the same performance as neural networks trained on the individual data sets. The ability of the neural network to generalize, producing algorithms with some degree of universality among diverse coastal environments, is thereby demonstrated. The result of the generalization analysis is of practical importance because it indicates that the neural network may not require an extensive training set of water depth data to be "tuned" for each location where depth retrievals are desired.

The work reported here addresses only the retrieval of water depth from remote measurements of spectral radiance. A similar approach is being followed leading to algorithms for retrieval of absorption and scattering coefficients of the water column and for classification of bottom types. Neural networks are emerging as an excellent methodology to serve as a basis for algorithms for these parameters in coastal waters where the complexity of the environment precludes use of less powerful approaches. Continued research into neural network based algorithms is recommended in preparation for the Navy Earth Map Observer satellite to be launched in the year 2000.

BATHYMETRY FROM HYPERSPECTRAL SENSORS: A PRELIMINARY ANALYSIS OF THE PROBLEM

INTRODUCTION

Optical remote sensing techniques have been employed by many investigators to derive information on the coastal marine environment. The most difficult aspect of this problem is the tendency of variations arising from changes in water depth, bottom type, and scattering and absorption in the water column (by chlorophyll, suspended sediments, colored dissolved organic matter, etc.) to be indistinguishable. A number of models or assumptions have been invoked to deal with this problem. Jerlov (1976) proposed a single-band model that assumes bottom reflectance and water attenuation are constant throughout the scene. Under these assumptions, reflectance in a single band can be related to water depth. However, these assumptions are hard to justify in practical situations. Polcyn and Sattinger (1969) were among the first to propose multibanded methods. Their two-band reflectance model assumes that there are two spectral bands in which the ratio of reflectance for all bottom types is the same and the ratio of water attenuation in the two bands is also constant. The band ratio model is not as restrictive as the single-band model. The two-band model allows bottom reflectance and water column attenuation to vary in magnitude as long as they are constant in spectral ratio. Paredes and Spero (1983) show that if there are as many spectral bands of data available as there are bottom types, depth retrievals can be achieved with total independence from multiple bottom types. The work of Paredes and Spero (1983) notwithstanding, methods for deriving bathymetry from multispectral data generally incur problems when the bottom reflectance varies appreciably (Nordman et al. 1990; Jupp 1988).

Multispectral extraction of water depth has been demonstrated with the Landsat Thematic Mapper (TM). Bands 1, 2, and 3 of the TM have water penetration capabilities. For example, Bierwirth et al. (1993) apply a multibanded model to the extraction of water depth and bottom reflectance from Landsat TM imagery. Their method assumes homogeneous water properties and some area in the scene where depth varies over a uniform bottom. The existence of a deep-water area in the scene where scene radiance is free from bottom effects is also required. The Bierwirth et al. (1993) method applied to Shark Bay in Western Australia resulted in a bias of several meters with the Landsat retrieval being too deep. Some investigators have used original Landsat bands for bathymetry, while others have performed various spectral transformations in an attempt to isolate the bathymetry contribution to the multispectral signal. For example, Walker and Kalcic (1994) used Gram-Schmidt orthogonalization of Landsat bands. Khan et al. (1992) used Principal Components Analysis. Lyzenga (1985) describes a combined lidar and passive multispectral scanner system for coastal bathymetry. The lidar system gives accurate depths at locations where the laser is fired into the water. The multispectral scanner uses the laser points for "calibration" to remove variability in bottom reflectance and water optical properties from multispectrally determined depth values in areas between laser soundings.

With the advent of hyperspectral scanners that sample the upwelling radiance spectrum in several tens of bands that have water penetration, more spectral discrimination power can now be brought to bear on the coastal optics problem. This report investigates relationships between hyperspectral radiance and water depth. The hypothesis explored is that the additional spectral bands available from a hyperspectral system will allow the bottom type, water optics, and depth variables to be unscrambled better than was possible with multispectral systems. AVIRIS (Airborne Visible/Infrared Imaging Spectrometer), an Earth-observing, imaging spectrometer sponsored by the National Aeronautics and Space Administration (NASA) and designed, built, and operated by the Jet Propulsion Laboratory, is well suited to this task. AVIRIS measures total upwelling radiance over the 0.4 to 2.4 mm spectral range in 224 channels spaced at 10-nm intervals. Images are about 11 km wide by up to 100 km in length with 20 × 20-m spatial resolution (Chrien et al. 1990; Vane et al. 1993). AVIRIS data were initially used in geology, vegetation studies, ecology, and other land-based remote sensing applications (Vane and Goetz 1993). An ongoing series of sensor improvements in SNR have made AVIRIS increasingly attractive for coastal oceanography. Carder et al. (1993) discuss the use of AVIRIS in the coastal oceanic environment. Hamilton et al. (1993) have related bathymetry of Lake Tahoe to upwelling spectral radiance recorded by AVIRIS using a multiple linear regression model.

This report examines the use of hyperspectral sensors to retrieve coastal water depth. The strengths and weaknesses of the available methods are examined and certain questions such as how many spectral bands, spectral placement of bands, and expected accuracies are examined. Recommendations for future Navy use of these systems and methods are included.

DATA SETS

Hyperspectral Imagery

AVIRIS data used in this study were collected on the western coast of Florida around Tampa Bay (Fig. 1) and in the Florida Keys between Upper Matecumbe and Plantation Keys (Fig. 2). The Tampa Bay image was collected on 5 Jun 1993 at 0810 LMT, and the Keys image on 23 Mar 1996 at 1256 LMT. The AVIRIS is flown aboard the NASA ER-2 aircraft at a nominal altitude of 20 km. A nautical chart (NAD 1983 datum) was digitized for each area and land points that were identifiable on both the AVIRIS image and the map were visually selected. These map/image matched pairs were used to form a two-dimensional polynomial function that was applied to the image to geometrically transform it to the map scale and projection. Image sample and line coordinates could then be related to latitude and longitude so that ground-truth depth observations could be associated with an AVIRIS pixel. The AVIRIS data were calibrated in units of radiance but were not corrected for atmospheric, ocean surface, or illumination effects. That is, retrieval of water depth was attempted from radiance values observed at flight altitude.

The absorption coefficient of water is quite high outside of the visible part of the spectrum. Therefore, only the 36 AVIRIS bands in the 400 to 742 nm range were expected to have sufficient water penetration to contain the bottom-reflected energy required for depth retrieval. Since the AVIRIS data were not atmospherically corrected, five additional bands were included in the data set to provide the neural network with atmospheric information. The atmospheric bands included are centered at 867, 943, 1020, 1136, and 1203 nm. All signals from these five bands can be considered to be of atmospheric origin or reflected from the ocean surface because the high values
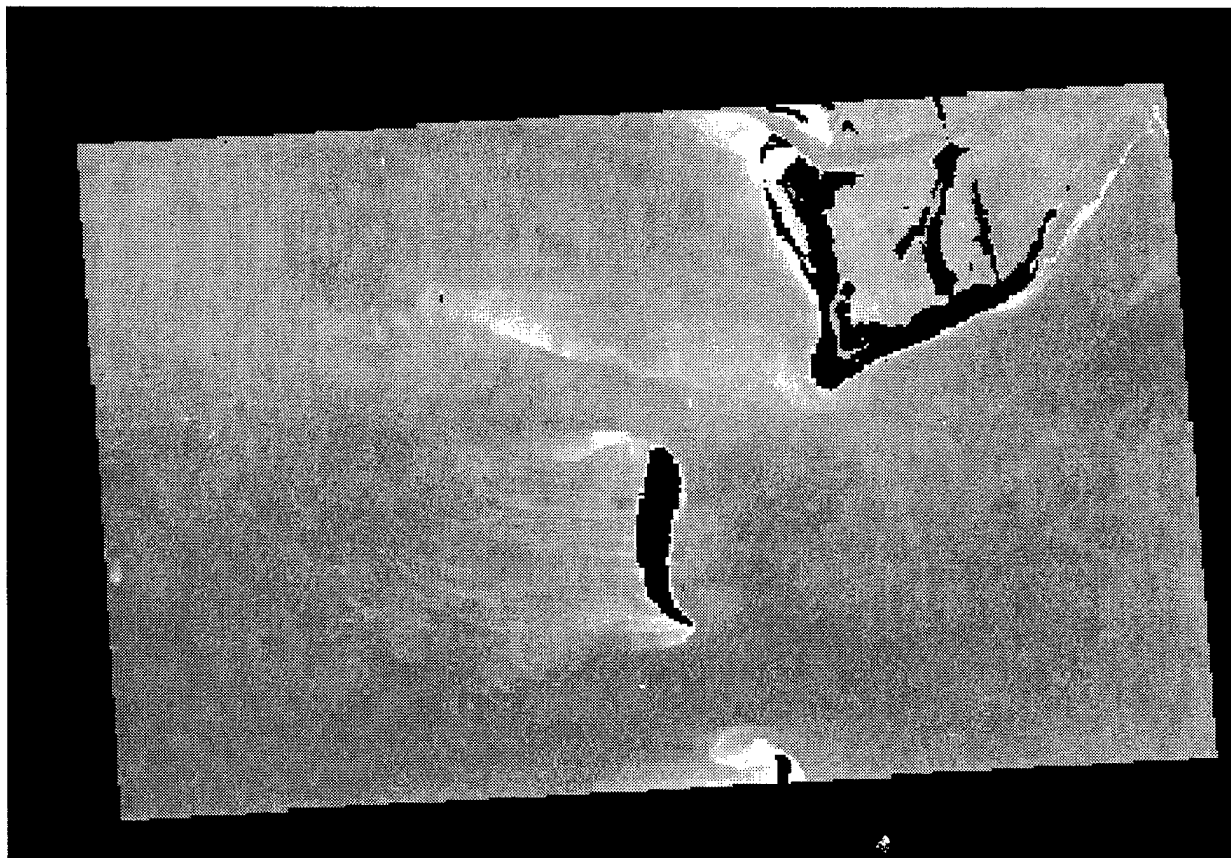
Fig. 1 – AVIRIS image (band 24, 606.5 nm) of the Tampa Bay area. Land areas denoted in black are Mullet Key (upper right), Egmont Key (center), and Passage Key (bottom edge). The image is a composite of two AVIRIS scenes.

of water absorption at these wavelengths preclude significant backscatter of light from within the sea. A total of 41 AVIRIS bands (36 water-penetrating and five atmospheric) were utilized in this study.

Bathymetry Data

The ground-truth data used in this study were soundings from the National Ocean Survey (NOS) hydrographic data base combined with sounding data collected by the Naval Research Laboratory (NRL). This study focused on retrieval of water depths ranging from 0 to 6 m. The 6-m limit was invoked because of the combined effects of the optical properties of the water column and the bottom reflectance at the study sites. Measurable levels of reflected energy from the ocean floor are required to perform an optical retrieval of depth. Subjective analysis of the AVIRIS images indicated that the absorption and scattering of the water column and the reflectance of the bottom combined to limit significant bottom-reflected radiance to locations where the water depth was less than 6 m.

For the area covered by the Tampa Bay scene, the NOS archive contained 11,067 bathymetry measurements of less than 6 m, which were used to form training and test sets for algorithm development. The soundings were collected from 1952 through 1995. All soundings were corrected to the NAD83 datum for direct comparison with AVIRIS images and nautical charts. The NOS archive contained some soundings that were relative to Mean Lowest Low Water (MLLW) and
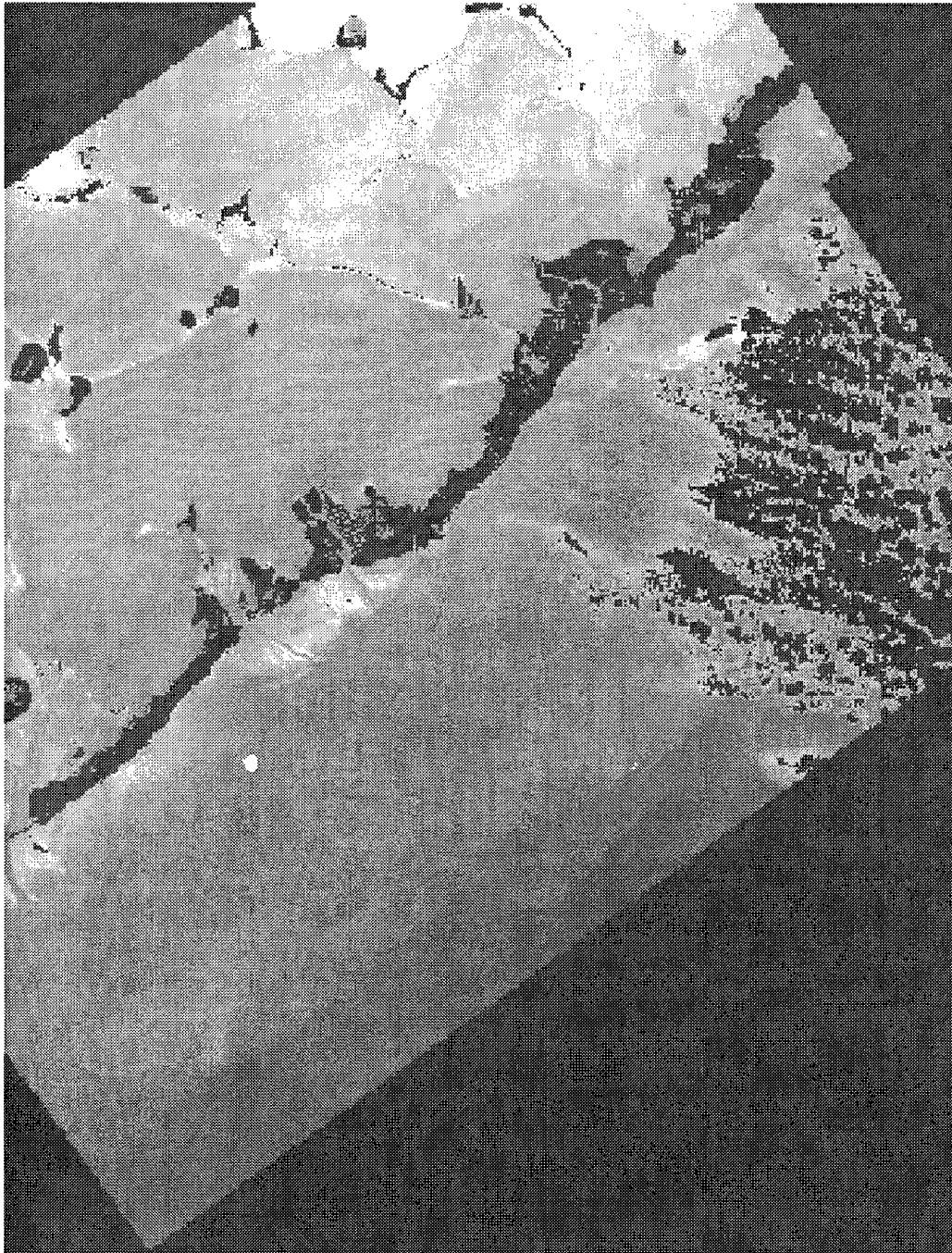
Fig. 2 – AVIRIS image (band 24, 606.5 nm) of the Florida Keys. Land areas denoted in black are Upper Matecumbe Key and Plantation Key. Black areas in the lower right corner of the image are clouds that have been masked in black. The image is a composite of six AVIRIS scenes.

others that were relative to Mean Low Water. The relationship between these two reference levels is complex and conversion from one to the other is not straightforward. Fortunately in the Tampa Bay area, the difference is typically on the order of 0.1 m. Therefore, no conversion was applied and the two reference levels were considered equivalent. Figure 3 shows the ground-truth sounding locations (0 to 6 m) as dots plotted over the image of Fig. 1. Figure 4 is a ground-truth depth image produced by resampling the ground truth (including depths >6 m) and encoding depth as grayscale.

Fig. 3 – Image of Fig. 1 with locations of NOS soundings in the range of 0 to 6 m marked with dots.

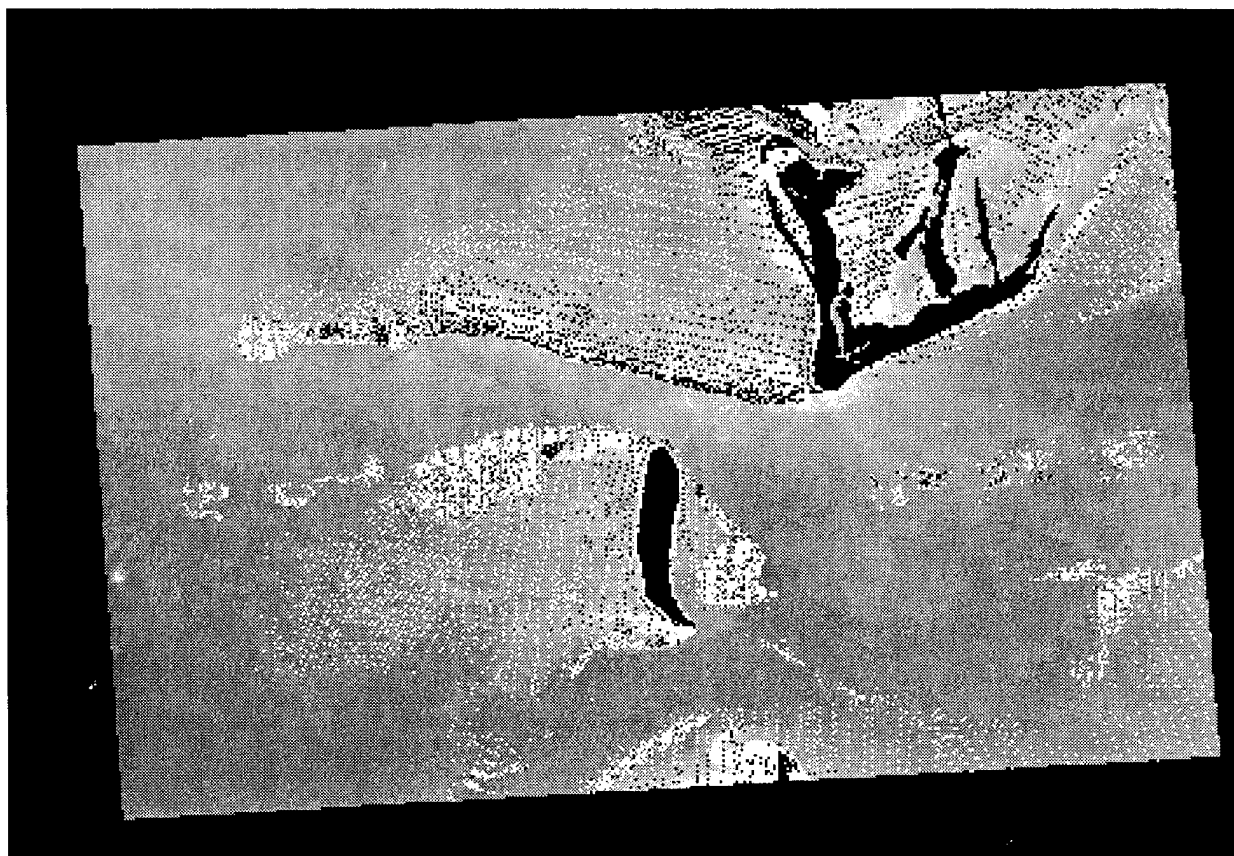The bottom configuration in an area such as the mouth of Tampa Bay changes in response to forcing by tidal and storm-generated currents, as well as the result of dredging. The ground-truth data is expected to show significant departures from the bottom configuration at the time of the AVIRIS overflight. The reader is reminded that the data considered to be "truth" in this case may contain significant errors because of the temporal mismatch with the AVIRIS image.

The Keys study area contains 46,435 NOS bathymetry measurements collected between 1934 and 1963. Because of the age of the NOS ground truth here, NRL collected 82,805 soundings of less than 6 m for the Keys site in August 1997. Positions of the NRL data are shown in Fig. 5. The NRL soundings were corrected to MLLW based on predicted tides at the time of observation. If actual tides differed from predicted tides, the difference would be a source of error in the Keys ground-truth data. Only the NRL soundings were used as ground truth for training and testing of the neural network algorithms. The Keys ground-truth data were, therefore, collected within 17 mo of the AVIRIS image.

Since no major hurricanes struck the Keys during this period, the ground truth in this case should contain smaller bottom change effects than did the Tampa data set. The NRL and NOS soundings were combined to produce the ground-truth depth "image" for the Keys site shown in Fig. 6. Note that the NRL survey lines in some cases can be seen in the depth image as dark lines. This indicates that the NRL survey produced deeper values than the NOS archive in these areas.
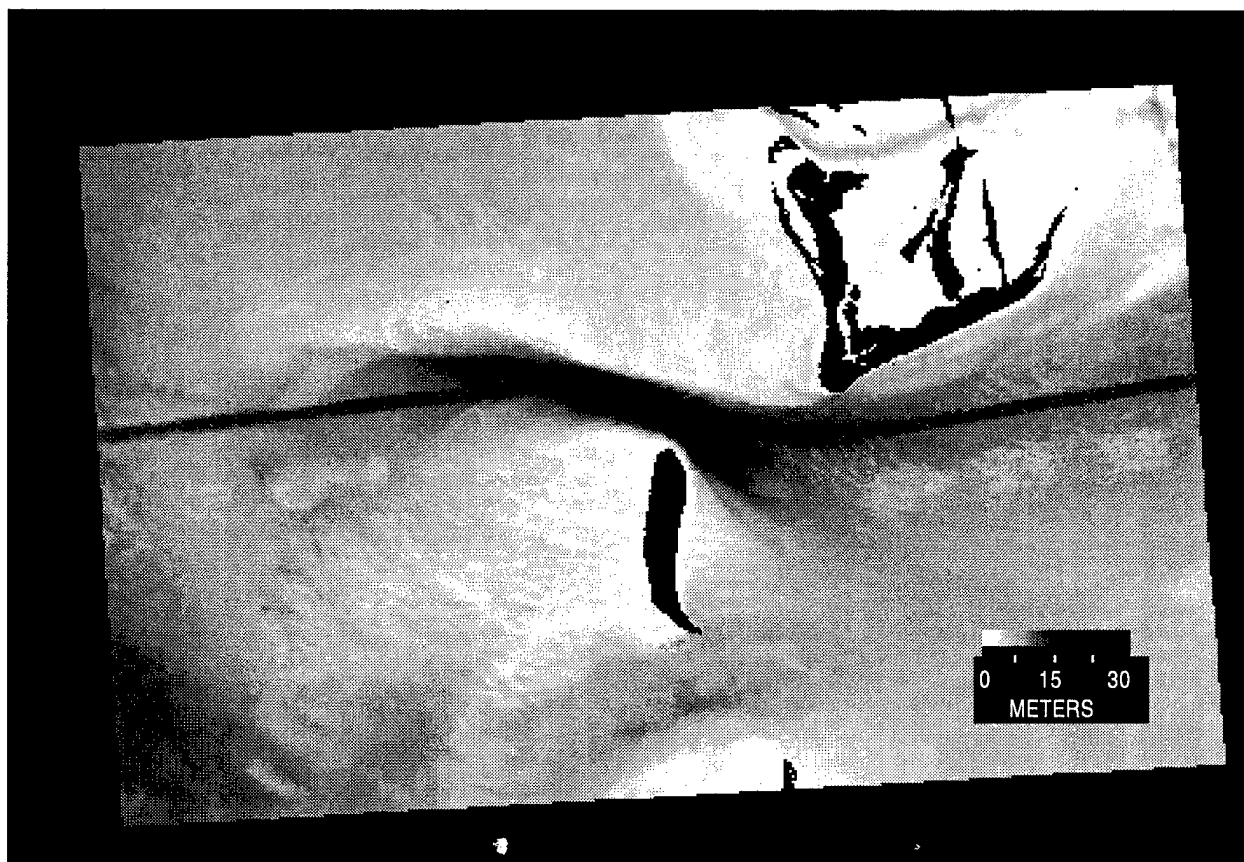
Fig. 4 – Tampa Bay ground-truth depth "image" produced by resampling ground-truth data onto the pixel grid of Fig. 1

THEORY

Radiative transfer in the coastal ocean/atmosphere environment is complex. Simplifications and approximations are generally required to make the problem tractable. The theory presented here is of this simplified form. The following is presented only to provide the reader with a conceptual framework for comparing various approaches to development of algorithms for the retrieval of coastal water properties (specifically water depth) from remotely sensed optical data. A rigorous treatment of radiative transfer in natural waters can be found in Mobley (1994).

Irradiance of the Sea Surface

Let E be the symbol for irradiance of a surface where irradiance is defined as the radiant flux impinging on the surface. Units of irradiance are energy per unit area. Irradiance of the sea surface is from two sources, direct sunlight E_{sun} and skylight E_{sky}. Skylight is the result of the scattering of sunlight by gaseous molecules (Rayleigh scattering) and by particles (Mie scattering) within the atmosphere. The total downwelling irradiance just above the air-water interface, $E^{+}\downarrow$, is then given by the sum of these two terms

$$E^{+}\downarrow = E_{sun} + E_{sky} . \tag{1}$$
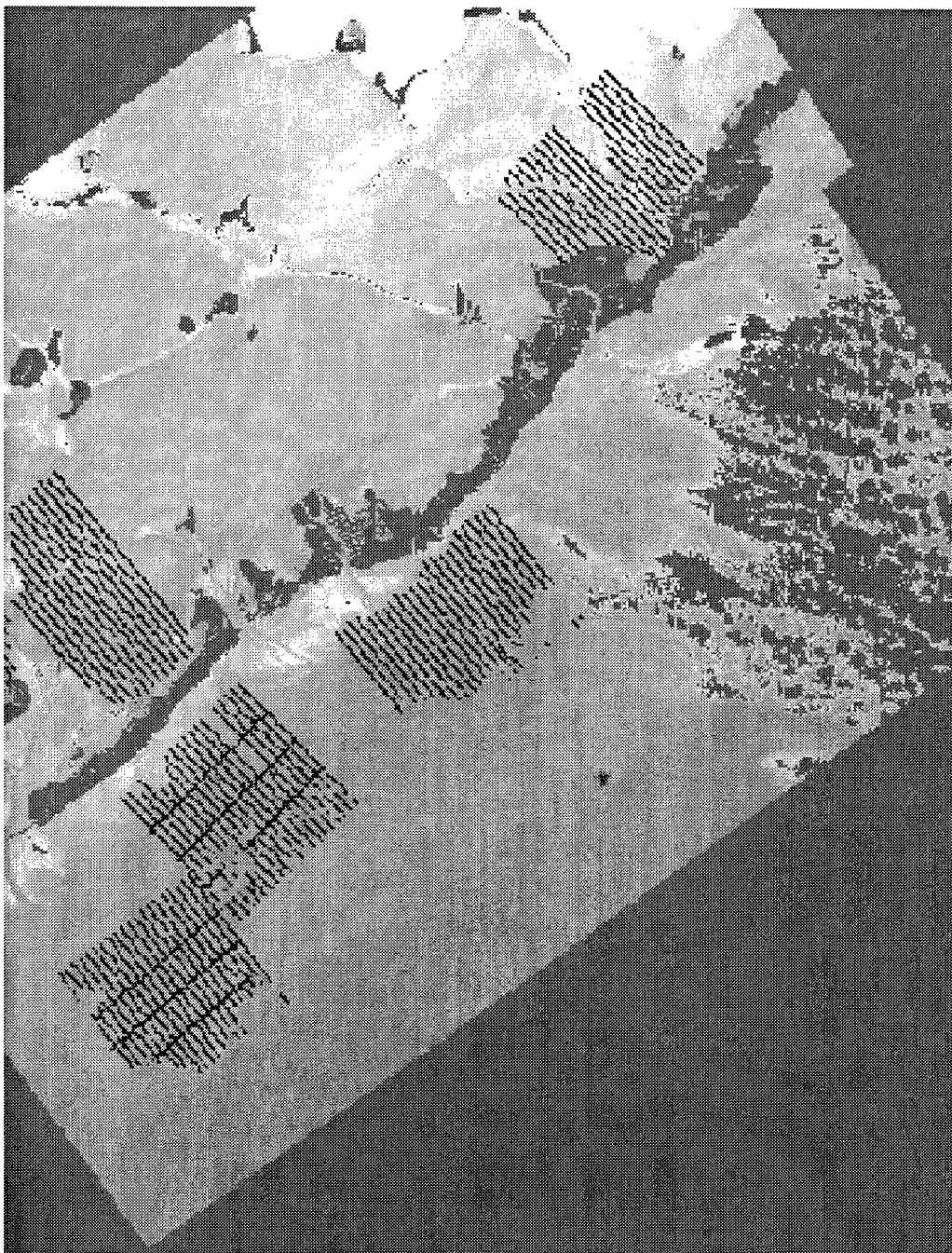
Fig. 5 – Image of Fig. 2 with locations of NRL soundings in the range 0 to 6 m marked
with dots

The irradiance terms E_{sun} and E_{sky} are not independent variables. Increased atmospheric scattering results in increased E_{sky}; hence, decreased E_{sun}. Irradiance from direct sunlight is unidirectional, striking the surface at angle θ with respect to vertical. Skylight, on the other hand, is angularly distributed as a function sun angle, the spatial distribution of atmospheric particulates (also called aerosols), and any fractional cloud cover that may be present.

The transmittance and reflectance of irradiance by the sea surface are the next factors to be considered. Surface-reflected light represents a signal to the sensor that is unrelated to water optics
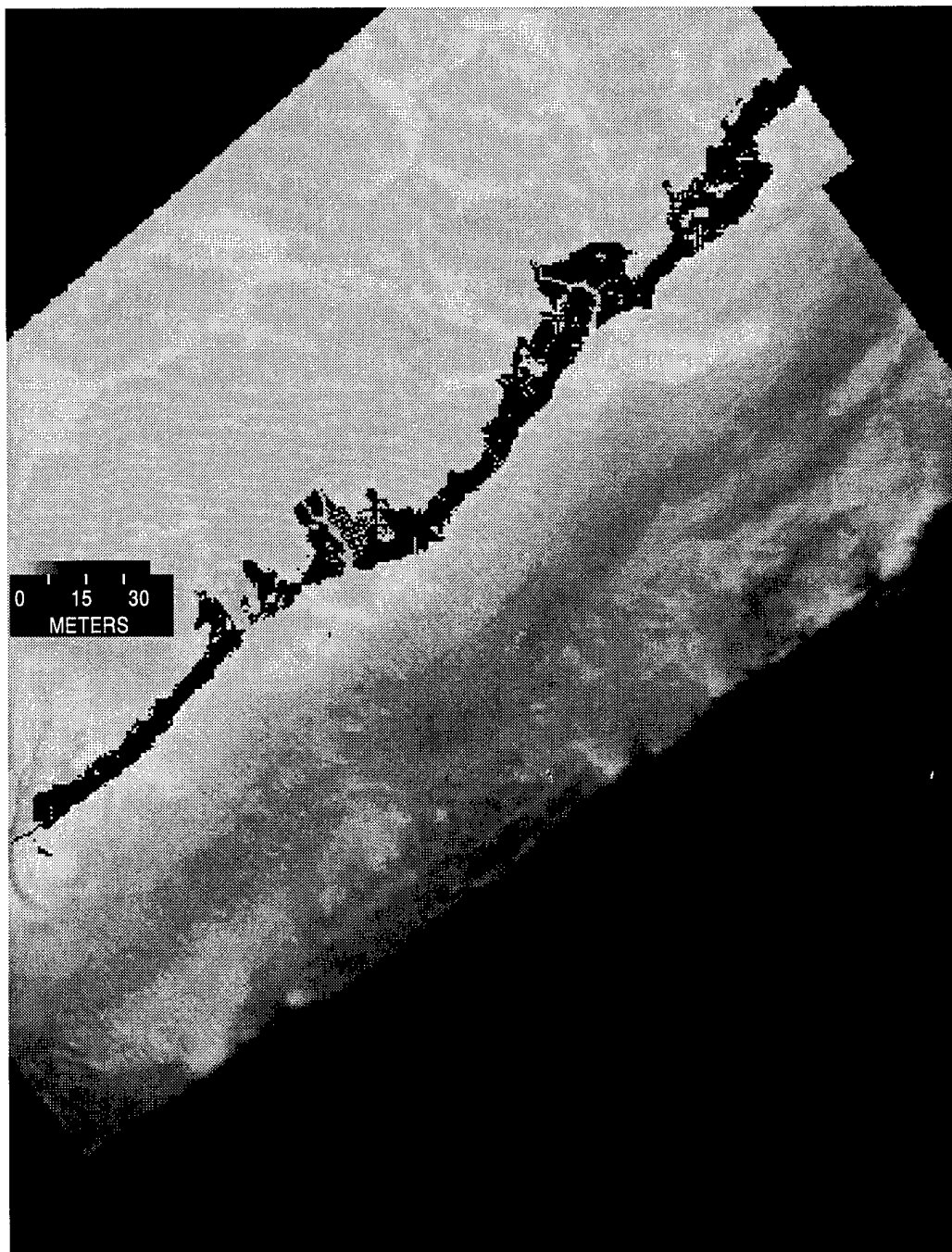
Fig. 6 – Keys ground-truth depth "image" produced by resampling ground-truth data (NOS and NRL) onto the pixel grid of Fig. 2

and must be removed to properly retrieve water optical properties from the remotely sensed data. The transmittance of the sea surface determines the fraction of surface irradiance that enters the water column and is available for in-water scattering and absorption. Conservation of energy requires that the reflection coefficient, r_{surf}, and transmission coefficient, t_{surf}, must sum to unity, i.e., the energy reflected by the surface and the energy transmitted through the surface must equal the total incident energy,

$$r_{surf} + t_{surf} = 1 \ . \tag{2}$$

The reflectance (transmittance) of light by a smooth sea surface is a function of incidence angle and polarization. Solar light is predominately unpolarized and its reflection coefficient can be assumed to be in the range of 0.020 to 0.025 for typical midday solar zenith angles. Since skylight is omnidirectional, the overall reflectance of skylight is an integral of reflected irradiance over the sky hemisphere. If the skylight is unpolarized and uniform in all directions, the value of the aforementioned integral yields a skylight reflectance of 0.066 (Apel 1987). The total reflection/transmission of surface irradiance, therefore, depends on the relative amounts of sunlight and skylight contributing to the surface irradiance. The sun and sky components will be treated individually here so that the downward irradiance just below the air-water interface, $E^-\downarrow$, is given by

$$E^-\downarrow = 0.98\, E_{sun} + 0.93\, E_{sky}\,. \tag{3}$$

Reflected and Backscattered Light from Within the Sea

The radiant energy that penetrates the sea surface and propagates downward through the water column can again reach the sea surface by one of two mechanisms. The downwelling energy can be backscattered to the surface by constituents in the water volume or it can be reflected to the surface from the seafloor. Of course, not all energy entering the sea returns to the sea surface since both the water column and the seafloor will absorb as well as backscatter and reflect photons. That energy returning to irradiate the air-sea interface from below, $E^-\uparrow$, then consists of two terms, $E^-_{vol}\uparrow$ and $E^-_{bot}\uparrow$, representing water volume backscatter and bottom reflectance, respectively,

$$E^-\uparrow = E^-_{vol}\uparrow + E^-_{bot}\uparrow\,. \tag{4}$$

Volume Backscatter

The volume backscatter coefficient b is the fraction of light in a beam incident upon a small volume element that is scattered at angles greater than 90° with respect to the beam. The beam backscatter coefficient accounts for loss of energy in the beam due to changes in the direction of propagation of the photons in the incident beam. Photons can also be lost by other mechanisms such as capture of photons by molecules and the subsequent conversion of radiant energy to thermal energy. The beam absorption coefficient a accounts for these dissipative losses. To a first approximation, $E^-_{vol}\uparrow$ can be expressed as a function of $E^-\downarrow$, a, and b (Apel 1987),

$$E^-_{vol}\uparrow = \frac{1}{3}\, E^-\downarrow \frac{b}{a}\,. \tag{5}$$

Note in Eq. (5) that larger beam backscatter coefficients lead to increases and larger beam absorption coefficients lead to decreases in irradiance of the underside of the sea surface from within the water volume.

Bottom Reflectance

Energy penetrating the sea surface propagates downward through the water column as a diffuse light field and is available to irradiate the seafloor. As depth of the bottom increases, bottom irradiance decreases because radiant energy is absorbed and backscattered by molecules and particles in the intervening water column. The rate of attenuation of the diffuse light field by the water column is called the diffuse attenuation coefficient K.

The seafloor is assumed to be a Lambertian reflector of light with reflectivity r_{bot}. Therefore, the light incident upon the seafloor is reflected back into the water column and propagates up through the water column, arriving as a diffuse light field irradiating the bottom side of the air-water interface. Since this upwelling irradiance just below the sea surface $E^-\uparrow$ has undergone two traverses of the water column and a bottom reflectance, its value just below the surface is given by

$$E_{bot}^-\uparrow = E^-\downarrow r_{bot} e^{-2Kd} .$$ (6)

Substituting Eqs. (5) and (6) into Eq. (4) gives the following expression for total irradiance of the air-sea interface from below

$$E^-\uparrow = E^-\downarrow \left(\frac{b}{3a} + r_{bot} e^{-2Kd} \right) .$$ (7)

Remote Sensing Considerations

The upwelling irradiance at the underside of the air-water interface is a multidirectional light field. This light is transmitted through the water surface where it is detected by a remote sensor observing from some specific angle. The angular nature of the observation requires that we consider radiance rather than irradiance as the light emerges from the sea surface. Radiance is in units of energy per unit area per unit solid angle. For a Lambertian surface, where radiance is uniformly distributed over the hemisphere, radiance L is related to E by

$$L = \frac{E}{\pi} .$$ (8)

If near normal viewing of the sea surface by the sensor is assumed, the transmittance of the sea surface to the water leaving radiance can be taken as the near normal value of 0.98. Therefore, the water leaving radiance L_{water} is given by

$$L_{water} = \frac{0.98}{\pi} \left[E^-\downarrow \left(\frac{b}{3a} + r_{bot} e^{-2Kd} \right) \right] ,$$ (9)

or substituting Eq. (3) into Eq. (9)

$$L_{water} = \frac{0.98}{\pi} \left[\left(0.98\, E_{sun} + 0.93\, E_{sky} \right) \left(\frac{b}{3a} + r_{bot} e^{-2Kd} \right) \right] .$$ (10)

When viewing the sea surface from above, the sensor receives skylight reflected from the sea surface. If L_{sky} is the radiance of the sky, then the surface-reflected sky radiance is $(0.02\, L_{sky})$, and the total radiance of the sea surface, L_{sea}, is given by

$$L_{sea} = \frac{0.98}{\pi} \left[\left(0.98\, E_{sun} + 0.93\, E_{sky} \right) \left(\frac{b}{3a} + r_{bot} e^{-2Kd} \right) \right] + 0.02\, L_{sky} .$$ (11)

Note in Eq. (11) that there is no term for surface-reflected sunlight. This omission is the result of the assumption that remotely sensed sea surface imagery is collected under conditions (time of day, geometry, etc.) such that no sunglint is imaged.

In remote sensing, the sea surface is viewed from an airborne or spaceborne platform that forces one to account for atmospheric effects on the signal from the sea surface. The atmospheric effects are the result of many complex factors and modeling of radiative transfer within the atmosphere is a separate discipline that can be avoided here by parameterizing the atmospheric effect as a transmission term, τ_{atm}, and a path radiance term, L_{atm}. Path radiance is light scattered by the atmosphere into the sensor field of view. Path radiance is, therefore, an additive term to the sea radiance of Eq. (11). Atmospheric transmittance is the attenuation of surface-leaving energy by scattering and absorption as it travels the atmospheric path to the sensor. Both L_{atm} and τ_{atm} are functions of the sensor look angle because off-normal viewing is through a longer path length than normal viewing. However, the assumption of near-normal viewing has already been asserted, so view angle dependency of L_{atm} and τ_{atm} can be ignored. The radiance of the sea surface as viewed from a sensor at altitude is, therefore, given by

$$L_{sensor} = \tau_{atm} \left[\frac{0.98}{\pi} \left[\left(0.98\, E_{sun} + 0.93\, E_{sky} \right) \left(\frac{b}{3a} + r_{bot} e^{-2Kd} \right) \right] + 0.02\, L_{sky} \right] + L_{atm} . \tag{12}$$

The substitution

$$E_{sun} = \tau_{atm}\, F_{sun} \cos\theta \tag{13}$$

can be made in Eq. (12) to give solar irradiance of the sea surface in terms of the solar flux above the atmosphere, F_{sun}, the atmospheric transmittance, τ_{atm}, and the solar zenith angle, θ. Several computer codes such as LOWTRAN and MODTRAN are available to calculate the atmospheric parameters L_{atm} and τ_{atm} if atmospheric data is known. Equation (14), therefore, represents a complete, albeit simplified, forward model that can be used to calculate observed radiance given the relevant parameters summarized in Table 1,

Table 1 — Summary of Variables from Equation (14)

Factor	Parameter	Description
Sun	F_{sun} θ	Solar Flux in Space Solar Zenith Angle
Atmosphere	L_{sky} τ_{atm} L_{atm} E_{sky}	Sky Radiance Atmospheric Transmittance Atmospheric Path Radiance Sky Irradiance
Water	d a b K	Water Depth Beam Absorption Coefficient Beam Backscatter Coefficient Diffuse Attenuation Coefficient
Bottom	r_{bot}	Ocean Bottom Reflectance

$$L_{sensor} = \tau_{atm} \left[\frac{0.98}{\pi} \left[\left(0.98 \left(\tau_{atm} F_{sun} \cos \theta \right) + 0.93 \, E_{sky} \right) \left(\frac{b}{3a} + r_{bot} e^{-2Kd} \right) \right] + 0.02 \, L_{sky} \right] + L_{atm} \, . \quad (14)$$

The simplifications and approximations implicit in Eq. (14) are highlighted below:

1. Sunlight and skylight are unpolarized.

2. Solar zenith angle is small.

3. There is no fractional cloud cover in the scene.

4. The sea surface is smooth (wind roughening and white capping are ignored).

5. Fluorescence is ignored.

6. A simplified *b/a* relationship is assumed for volume reflectance of the water column.

7. The seafloor is assumed to be a Lambertian reflector.

8. The water column is vertically homogeneous, i.e., *K*, *a*, and *b* are not functions of depth.

9. The exponential form of attenuation of the diffuse light field infers that multiple scattering has been ignored.

10. Upwelling light from the water column that has been reflected back into the column by the water surface has been ignored.

11. Remotely sensed sea surface imagery is collected under conditions (time of day, geometry, etc.) such that no sunglint is imaged.

12. The sky is of uniform radiance from horizon to horizon.

Though the above assumptions and approximations have gone into the formulation of the forward problem shown as Eq. (14), the derived relationships are complex. L_{sensor} could, in principle, be calculated from Eq. (14). However, the remote sensing problem, i.e., given L_{sensor}, calculate *d*, *K*, or r_{bot} is not a tractable problem since we have a single equation in 11 unknowns. Possible methods for the inversion of Eq. (14) to obtain water depth, d, from airborne observations of Latm are the topic of this report, but similar methods and discussion could be directed toward the retrieval of other geophysical parameters such as *K*, *a*, *b*, or r_{bot}.

INVERSION FOR BATHYMETRY

Approach

The problem at hand now is to solve Eq. (14) for water depth given an observation of ocean radiance from a spaceborne platform. Since there are 11 variables in Eq. (14), it will be necessary to make additional assumptions, approximations, and image-based calculations or to have independent knowledge of some of the parameters to simplify Eq. (14) to the point where L_{sensor} is, in effect, calibrated in units of water depth. An example of this approach can be found in Bierwirth et al. (1993). Development of an algorithm of this type follows.

Start with the assumption that none of the variables in Eq. (14) are functions of position within the image. That is, the water, the ocean bottom, and the atmosphere are horizontally homogeneous. This assumption allows one to determine one of the required variables at one location in the image and apply that value to any other pixel in the scene.

Further, assume that bathymetry retrieval will only be possible where the water is relatively clear. Mathematically, clear water means

$$\frac{b}{3a} \ll r_{bot}e^{-2Kd}, \tag{15}$$

so that

$$\left(\frac{b}{3a} + r_{bot}e^{-2Kd}\right) \cong r_{bot}e^{-2Kd}. \tag{16}$$

Another simplification of Eq. (14) results by assuming the equality of L_{sky}, the radiance of an atmospheric path from the Earth looking toward space, and L_{atm}, the radiance of an atmospheric path from space looking toward the Earth. Setting $L_{sky} = L_{atm}$ is reasonable if multiple scattering in the atmosphere is ignored and if the scattering phase function for atmospheric particulates are symmetrical in the upward and downward directions. If these three simplifications are incorporated into Eq. (14) and variables are grouped into constants, Eq. (14) can be written as

$$L_{sensor} = C_1 e^{-2Kd} + C_2, \tag{17}$$

where

$$C_1 = \tau_{atm}\left[\frac{0.98}{\pi}\left(0.98\left(\tau_{atm}F_{sun}\cos\theta\right) + 0.93\,E_{sky}\right)\right]r_{bot} \qquad C_2 = L_{atm}\left(1 + 0.02\,\tau_{atm}\right) \cong L_{atm}. \tag{18}$$

The constants C_1 and C_2 can be determined from a deep-water and a beach pixel in the remotely sensed image.

A deep-water pixel is selected where the value of d is very large. The deep-water pixel $L_{sensor} = C_2$ will be called L_{deep}. The deep-water radiance value is now subtracted from every pixel in the image. The resulting pixels are related to depth as

$$\left(L_{sensor} - L_{deep}\right) = C_1 e^{-2Kd}. \tag{19}$$

To evaluate C_1, a pixel is selected where the depth is 0, i.e., a beach pixel where the beach material is assumed to be the same as the ocean bottom material. The selected beach pixel should contain wet material since the seafloor is wet. The value in the beach pixel (after subtraction of the deep value) is C_1. This value of C_1 will be called $(L_{sensor} - L_{deep})_{beach}$. The equation relating observed radiances to depth for any other pixel now becomes

$$\left(L_{sensor} - L_{deep}\right) = \left(L_{sensor} - L_{deep}\right)_{beach}e^{-2Kd}. \tag{20}$$

The last step leading to a bathymetry algorithm is to determine a value of K in Eq. (6). This is possible if we know two different water depths within the image. Taking the natural logarithm of each side of Eq. (20) and rearranging terms results in

$$\ln\left(L_{sensor} - L_{deep}\right) = -2Kd + \ln\left(L_{sensor} - L_{deep}\right)_{beach} , \tag{21}$$

showing that K is related to the slope of a linear plot of $\ln(L_{sensor} - L_{deep})$ vs. d, which can be constructed from the observed radiances at the pixels of known depth. Specifically,

$$K = -\frac{1}{2}slope . \tag{22}$$

Depth can now be retrieved from the remotely sensed radiances by

$$d = \frac{1}{2K}\left[\ln\left(L_{sensor} - L_{deep}\right)_{beach} - \ln\left(L_{sensor} - L_{deep}\right)\right] . \tag{23}$$

Note that four additional assumptions or approximations given in the box below have gone into the derivation of the bathymetry algorithm given in Eq. (23). The accuracy of the depth retrievals from this method will depend on the extent to which these four factors, plus the 12 associated with the derivation of Eq. (14), are met in a given situation.

1. The seafloor, water column, and atmosphere are horizontally homogeneous.

2. Water is clear enough and shallow enough that bottom-reflected radiance is much larger than backscattered radiance from the water column.

3. Atmospheric haze is low enough that multiple scattering in the atmosphere can be ignored.

4. Depths (different values) are known at two points within the image.

(Assumptions and approximations required for retrieval of water depth from remotely observed radiance).

An Example

An AVIRIS image of Tampa Bay will be used to illustrate the use of Eq. (23) to retrieve water depth. Note that Eq. (23) is a "single-channel" algorithm using only one wavelength. Which of the spectral channels available from AVIRIS would be the best selection of a single channel? To answer that question, we note that depth is related to the logarithm of radiance. The linear correlation coefficient between depth and $\ln(L)$ has been calculated for each of the 41 AVIRIS spectral bands included in this study. The correlation calculations included the co-located depth/radiance pairs from both Tampa Bay and the Keys. Figure 7 shows the correlation value as a function of AVIRIS channel number. The highest correlation between the imaged radiance and depth is found in the AVIRIS channels 24 through 28. The high correlation values at these wavelengths indicate that if one could use only one band for a bathymetry algorithm, a band in this range would be the best choice (for West Florida and Keys waters). AVIRIS channel 24 centered at 606.5 nm (Fig. 1) has been selected to illustrate the single-band approach.

In Fig. 8, the location used as the deep-water radiance is shown by the (+) toward the left edge of the figure. The average scaled radiance value in the 10 × 10 box around the (+) is 879.7. The pixel assumed to contain moist sand to be used as the beach reference is located on the northern tip of Passage Key. The radiance value for the moist sand is 903.7. The astericks (*) near the
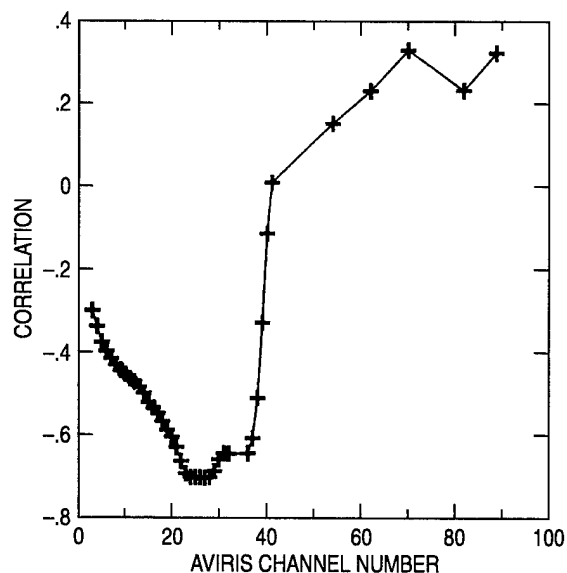
Fig. 7 – Correlation of depth with radiance as a function of AVIRIS channel number
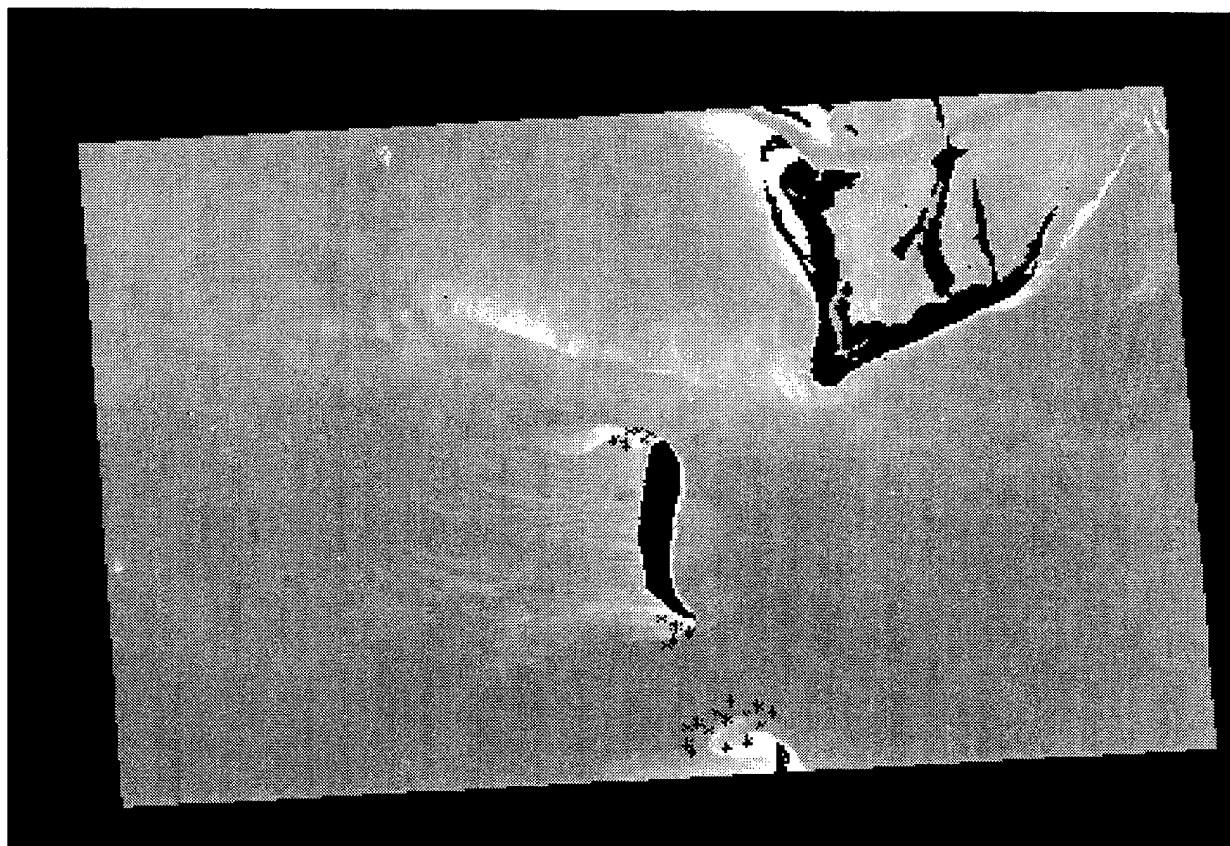
Fig. 8 – Figure 1 with points for multiple depths over a uniform bottom shown as astericks (*) and the deep-water reference point shown with a + symbol

northern end of Passage Key are locations where depth is known from the archives of the NOS and where we have assumed the bottom reflectance to be uniform. Figure 9 is a plot of the logarithm of deep-water, corrected radiances under the astericks vs. the NOS depth values. The data in Fig. 8 has been fit with a least-squares line, which is also shown in the figure. The slope of that line is
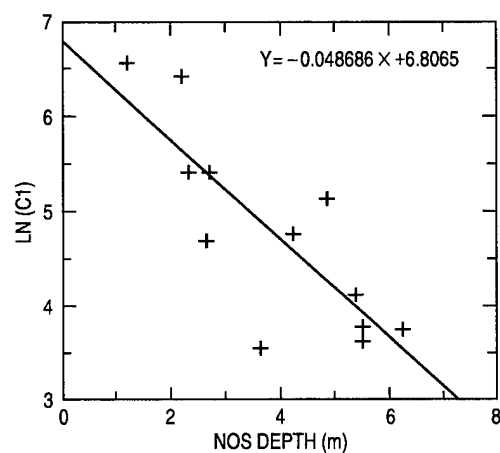
Fig. 9 – Plot of ln(L) vs. depth over the assumed uniform
bottom at the north end of Passage Key. Data points in
the plot were taken from the locations marked by astericks
(*) in Fig. 8.

Fig. 10 – Depth image produced by applying Eq. (23) to each pixel within Fig. 1

-0.048686, resulting in a K estimate of 0.024343 m^{-1} for the water in this scene. This value of K indicates an optical depth of approximately 41 m, which seems intuitively too high for waters on the west Florida shelf. This unexpected result is likely evidence that the assumptions associated with this method are not completely correct for this case. This K value has been inserted into Eq. (23), which is then applied to give a depth estimate for each pixel in the scene. The depth
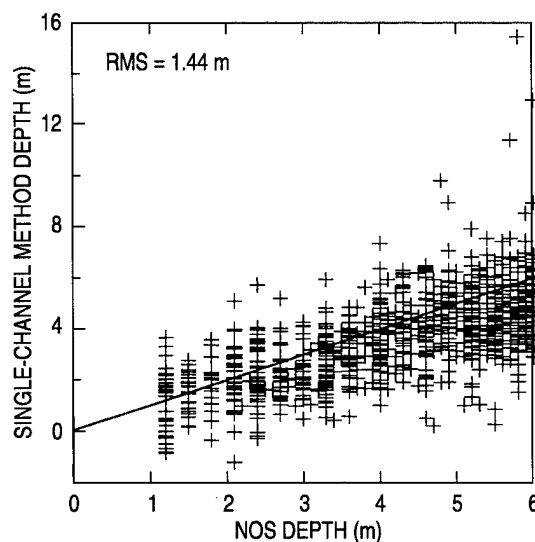
Fig. 11 – Single-channel estimated depth vs. NOS
values for the Tampa Bay test set

values are encoded as gray levels and displayed in image format so that Fig. 10 is a depth image of the AVIRIS scene produced by the single-channel algorithm of Eq. (23). The ground-truth bathymetry data set for Tampa Bay contains 923 soundings within the confines of the AVIRIS scene that can be compared to the values retrieved from Eq. (23) to give an estimate of the algorithm accuracy in this case. Figure 11 is a scatter plot of ground-truth depth value vs. the single-channel depth retrievals. The root-mean-squared (RMS) difference between these values is 1.44 m.

Note in Fig. 11 that not only is the scatter of points high, but a bias (to the deep side) is also present in the remotely sensed depth values. This bias was also reported by Bierwirth et al. (1993) who used an approach similar to that leading to Eq. (23). Also, note in Fig. 10 that depths in the upper half of the scene are much too shallow compared to the ground-truth depth image of Fig. 4. The explanation offered for this result is that the atmosphere over the scene was not horizontally homogeneous as the derivation assumed, but a cloud of aerosols was present in the top half of the scene that was not present in the lower half. The aerosol patch has resulted in anomalously shallow depth retrievals in this area. The large scatter and the bias in the error statistics and the aerosol-induced errors provide the justification for moving to a multibanded approach to depth retrieval.

BAND SELECTION

The single-band approach fails because there are many environmental factors and only one observation of radiance (mathematically speaking, one equation in many unknowns). This mathematical situation is not in general solvable; hence, the poor results produced by the single-channel bathymetry algorithm. By observing the upwelling radiance of the sea at multiple wavelengths, an equation like Eq. (23) exists for each wavelength. The bathymetry algorithm can now be formulated as a solution of simultaneous equations eliminating some of the unknowns leading to improved depth retrievals. However, in moving to a multispectral approach, the number of unknowns increases as well as the number of equations since variables like water column inherent optical properties and bottom reflectance assume different values at each wavelength. Actually, the number of variables increases faster than the number of equations so that no number of spectral bands will ever result

in an explicit mathematical representation for depth as a function of observed spectral radiance. The only factor that makes this problem mathematically tractable at all is the fact that the unknowns are not independent. Correlation between the unknowns means that there are truly fewer variables (in the mathematical sense) than there are unknowns in the simultaneous equations. The question then arises, how many spectral bands are required to perform the best possible retrieval of water depth from spectral radiance?

Many numerical methods exist for examining the number of bands required (the true dimensionality of the hyper-dimensional data set in mathematical terms). Principal Components Analysis (PCA) is one widely used method (Johnson and Wichern 1982). In PCA, the covariance matrix of the hyper-dimensional data set is formed and the eigenvalues and eigenvectors of the covariance matrix calculated. The eigenvectors represent a new set of basis functions that are oriented to capture variance in the data set while maintaining orthogonality with respect to each other. The eigenvalues associated with each eigenvector express the amount of data set variance in the direction of the eigenvector. If the eigenvalues are ranked by size, the summation of the first three eigenvalues divided by the summation of all eigenvalues gives the fraction of the total variance of the data set that can be preserved if the data set is reduced to three dimensions. Likewise, the sum of the first four eigenvalues compared to the sum of all eigenvalues indicates the fraction of the variance that can be contained in a four-dimensional coordinate system. The number of eigenvalues that must be summed to account for nearly all (say 95 or 99%) of the variance is often interpreted as the true dimensionality of the data set. Note that PCA involves a linear transformation of variables. It has been shown in previous sections that the depth-to-radiance relationship is exponential. The PCA transformation is, therefore, not optimal for this application. However, the objective here is an approximation to the dimensionality of the data set. PCA will be informative in this context, even though it is a linear analysis applied to a nonlinear problem.

The AVIRIS data sets for Tampa Bay and the Keys have been combined and submitted to PCA. The data analyzed are the spectral radiance values that are co-located with the depth ground-truth locations, a total of 93,872 data points. In this case, the original data set is 41-dimensional, since 41 AVIRIS channels have been used. The covariance matrix is then 41 × 41 and eigen analysis of that matrix results in 41 eigenvectors and their associated eigenvalues. Figure 12 shows the cumulative sum of eigenvalues divided by the sum of all eigenvalues as a function of number of eigenvalues included in the cumulative sum. The figure shows that 95% of the variance is contained within the first dimension and 99% of the variance within the first three dimensions. The conclusion from this result is that the 41-dimensional AVIRIS data set has a true dimensionality of approximate order 3. In other words, only three spectral bands at properly selected wavelengths would be required to extract all depth-related information from this AVIRIS data set. This dimensionality result is not universal. AVIRIS data from other locations may exhibit significantly different dimensionality. In general, the dimensionality of a hyperspectral image data set is expected to depend on the complexity of the scene. If there are many widely different bottom and water types within the scene, the dimensionality will increase. There is more to be said about band selection. For example, we have not identified what the wavelengths of this reduced subset of spectral bands should be. In addition, it could be argued that methods other than PCA would be more appropriate here for determination of true dimensionality. This topic will be addressed further in later sections. For now, we simply want to make note of the fact that the 41 channels sampled by AVIRIS represent a spectral oversampling. We proceed to work with all 41 channels in the following section where neural networks are utilized to develop quantitative relationships between spectral radiance and depth.
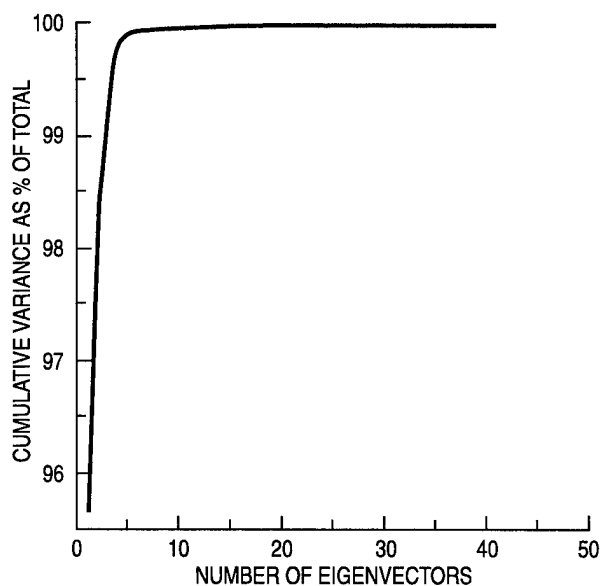
Fig. 12 – Cumulative variance vs. number of dimensions
for combined Tampa Bay and Keys training sets

NEURAL NETWORKS

A neural network is a parallel computing architecture that can be trained by supervised learning to perform nonlinear mappings, such as the mapping from spectral radiance to water depth (see Lippman (1987) for an introduction to neural networks). The processing conducted by each processing element (or neuron) in the network consists of forming a weighted sum of the inputs followed by a nonlinear transfer function to produce an output. The outputs thus produced by one layer of processing elements become the inputs to the next layer in the network. The "intelligence" in the network is contained in the weights that go into forming the sum in each processing element. The proper weights are established by supervised learning using input data vectors with known desired outputs. The neural network used in this study is a feed-forward, fully connected net with an input layer (41 neurons), one hidden layer (21 neurons), and an output layer containing a single neuron.

Supervised training is accomplished by back propagation, which iteratively presents spectral data as input and ground-truth depth as the corresponding desired output. Back propagation uses a gradient descent search technique to adjust network weights at each iteration to minimize the mean squared error between the desired output and the actual network output. The training should result in a network that produces least-squares estimates of depth given input spectra from the training set. The trained network is tested with an independent set of input data not included in the training process. Accuracy statistics cited in this report are for these independent test sets.

A characteristic of neural networks often cited to their credit is their ability to generalize. The network not only performs well on the training data, but often is able to solve related problems by generalizing training set relationships to slightly different problems. The ability of the neural networks trained here to generalize is an important factor. If generalization does not occur, then the network would need to be trained for each set of water/bottom/illumination conditions. If generalization does occur, then the network has learned general principles of radiative transfer in the coastal ocean, and bathymetry retrievals under conditions not explicitly included in the training procedure might be possible. A secondary objective of this study is to examine the generalization or the universality of the derived mappings of spectral radiance to water depth.

RESULTS

Training on Individual Data Sets

The neural network was trained on the Tampa Bay training set consisting of 10,144 samples, each sample being a vector containing the 41 AVIRIS radiance values recorded at the location of a ground-truth depth point. Depths in the test and training sets were corrected for predicted tidal height at the time of the AVIRIS overflight. If actual tides differed from predicted, errors of unknown magnitude were present in the training and test sets. Training proceeded for 4 million iterations at which point the neural network indicated convergence to a stable solution. After training, the neural network weights were fixed and the success of the training procedure was evaluated in two ways. First, the neural network was applied to vectors from an independent test set consisting of 923 samples. The RMS error between the depth estimated by the trained neural network and the NOS soundings for the Tampa Bay test set was 0.84 m over the 0- to 6-m range. Figure 13 is a plot of the neural network estimated values of depth vs. the NOS value for the test set. The second evaluation was to apply the neural network to the radiance vectors from each pixel in the image to produce an estimated depth for that pixel location. The estimated depths for all pixels were encoded as grayscale and displayed in image format. Figure 14 is the neural network estimated depth image for Tampa Bay. The neural network depth image compares favorably with the ground-truth depth image (Fig. 4). The spatial distribution of the errors can be examined by displaying the depth error value for each pixel (Fig. 14 minus Fig. 4) as the image shown in Fig. 15.

The same neural network training and testing procedures were applied to the Keys data set. In the Keys, the training set consisted of 74,524 samples and the test set of 8,281 samples. Test set RMS error for the Keys was 0.39 m over the range 0 to 6 m. Figure 16 is the error plot for the Keys test set, Fig. 17 is the neural network depth image, and Fig. 18 is the depth error image for the Keys.
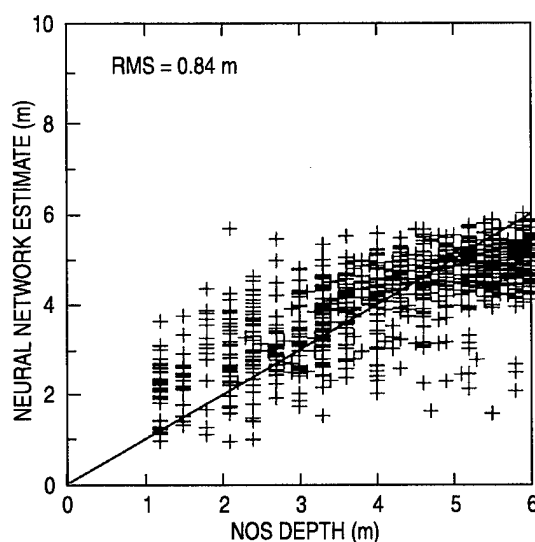

Fig. 13 – Neural network estimated depths vs. ground-truth values for Tampa Bay test set
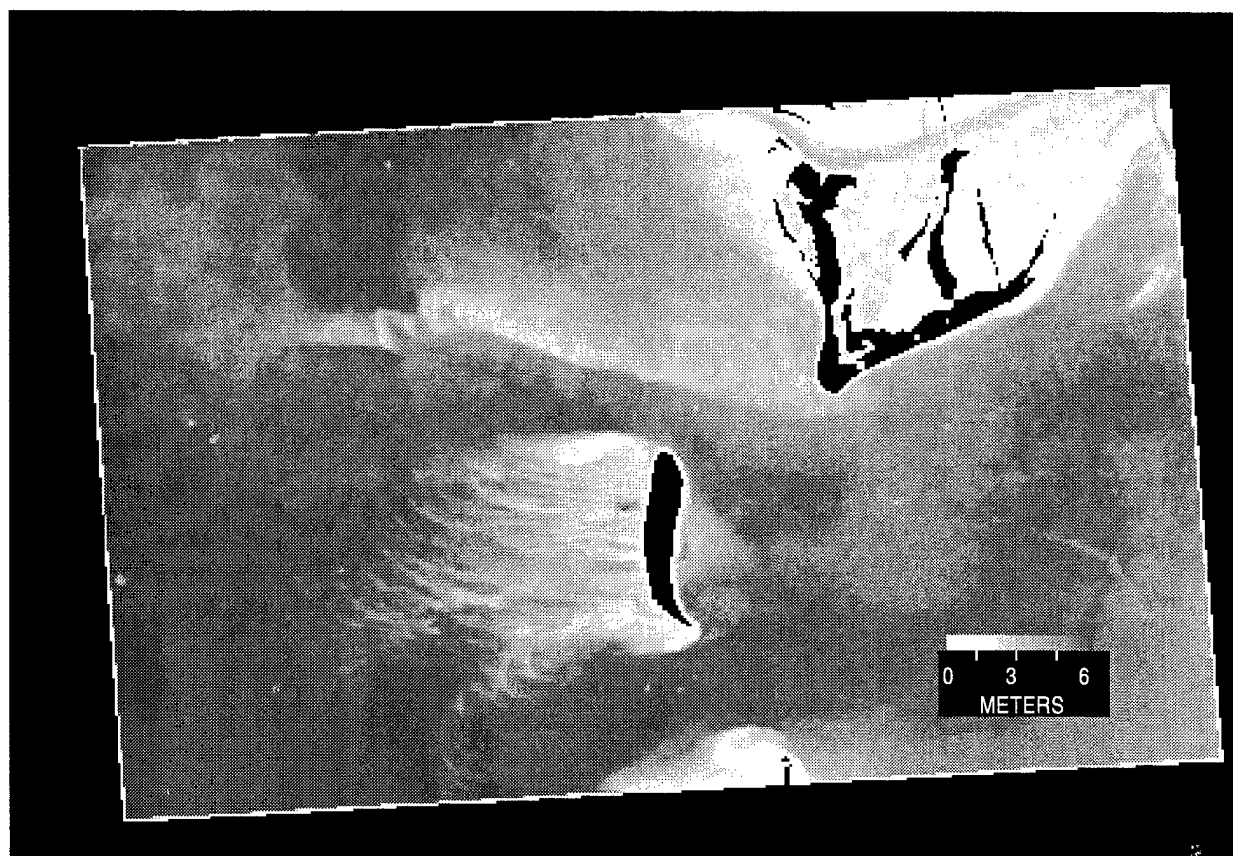
Fig. 14 – Tampa depth image produced by applying the neural network to each pixel in the Tampa scene

Training on Combined Data Sets

A key factor related to the value of the neural network approach is the degree to which universal network weights can be found that will permit depth retrievals for water and bottom types not explicitly contained in the training set. If neural network algorithms cannot be extended to new areas, complete retraining, requiring thousands of ground-truth points, would be necessary for every data set. To investigate this question, the Tampa and Keys training sets were combined to determine if the neural network could produce a single spectral radiance to depth mapping that would perform as well as the mappings generated by training on the individual data sets. These two data sets are from different seasons of the year as well as different locations, so a difference in water column properties is expected, although no optical ground truth was collected coincident with either of these flights. The Tampa Bay data was collected under summer conditions through a warm, maritime atmosphere. The solar elevation during the early morning flight was approximately 46°. AVIRIS imaged the Keys site in the spring of the year, closer to noon when the solar elevation was approximately 65°. The different solar elevations for the two cases would have resulted in different solar irradiance of the sea surface for each case. No normalization for differences in surface irradiance was applied to these data. The Keys site extended from clear offshore waters to the south to the more turbid waters of Florida Bay to the north. Although no bottom-type ground truth was collected, the Keys certainly contain coral that was not present at the Tampa site. These two data sets do represent variability in water types, bottom types, atmospheric conditions, and illumination levels and, therefore, present a challenge for development of a single algorithm that will produce reasonable depth retrievals for both cases.

Fig. 15 – Tampa Bay depth error image. Darker shades indicate areas where the neural network estimate is too shallow, lighter shades indicate areas where the neural network estimate is too deep

Fig. 16 – Neural network estimated depths vs.
NRL values for the Keys test set

The same training procedures were used on the combined data as were used for the individual cases. The neural network resulting from combined training resulted in an RMS error of 0.48 m when evaluated on a combined independent test set. Figure 19 is a scatterplot of the ground-truth depth vs. the neural network estimated depth for the combined test set. The combined algorithm resulted in an RMS error of 0.95 m when applied to the Tampa image. This compares with an RMS
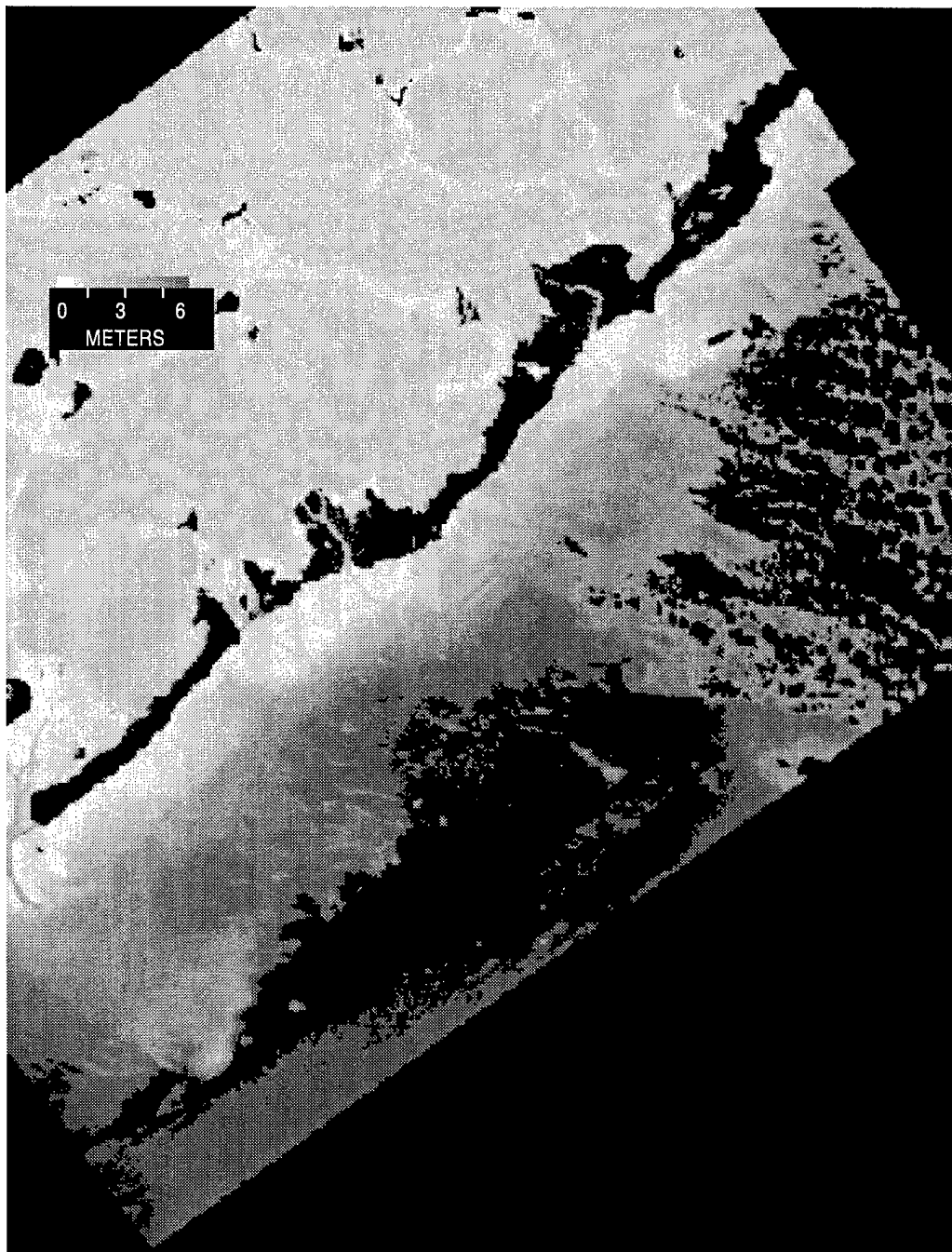
Fig. 17 – Keys depth image produced by applying the neural network to each pixel in the Keys scene

error of 0.84 m when the training included Tampa Bay only. Likewise, the combined algorithm resulted in an RMS error of 0.40 m when applied to the Keys test set, compared to 0.39 m when training included the Keys only.

DISCUSSION OF NEURAL NETWORK RESULTS

The depth retrievals from the Keys site were significantly more accurate than those from Tampa Bay. The larger errors for Tampa Bay can be attributed to two major causes. The first is

the large time separation between the ground-truth and the airborne data collections. Depths may have changed significantly between the ground and the airborne collections resulting in an unknown, but significant, portion of the Tampa Bay errors. The second factor is the signal-to-noise ratio (SNR) of the AVIRIS instrument, which has constantly improved during the AVIRIS lifetime. The SNR for the AVIRIS reference radiance at 608 nm (the approximate wavelength of maximum correlation of radiance to depth) was 923 during the 1996 collection in the Keys, but was only 535 in 1993 during the Tampa Bay experiment (Green 1998; Green et al. 1995). Hence, more accurate
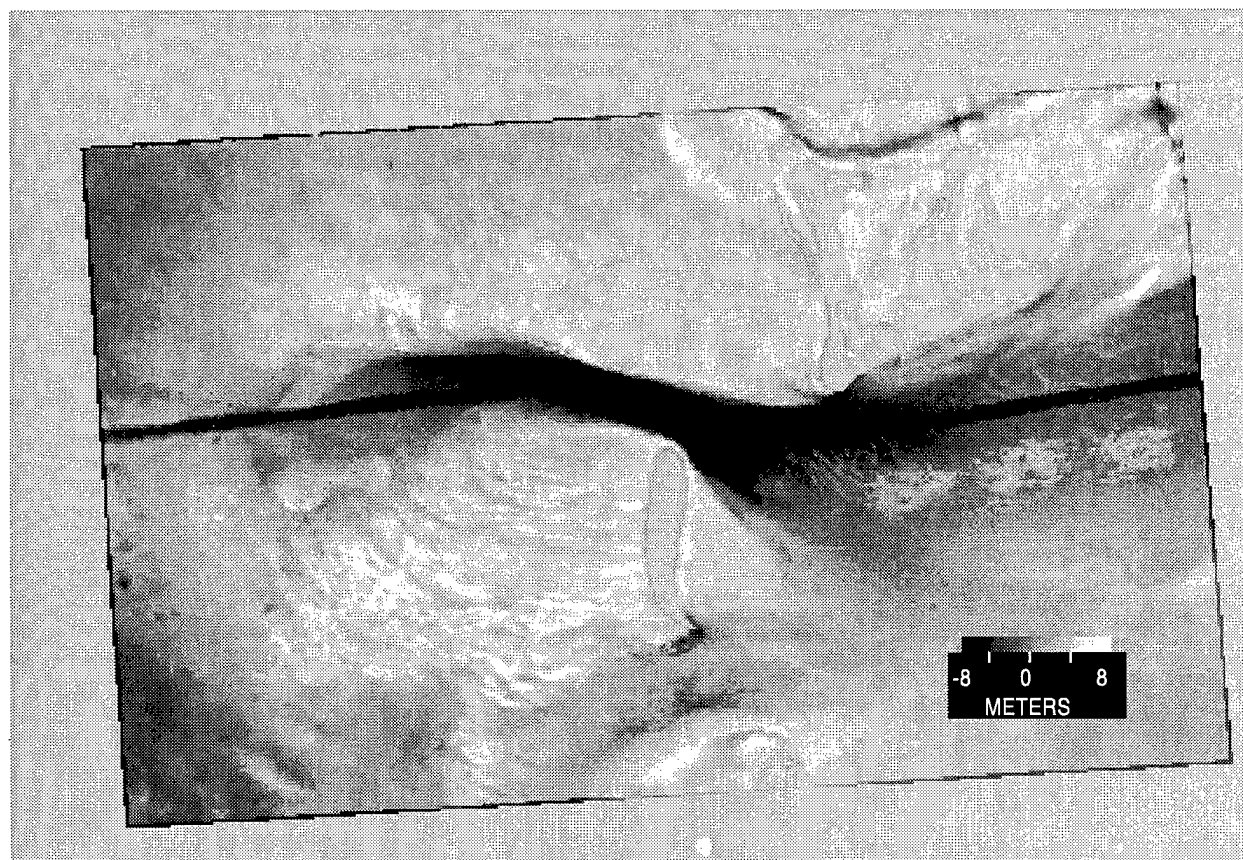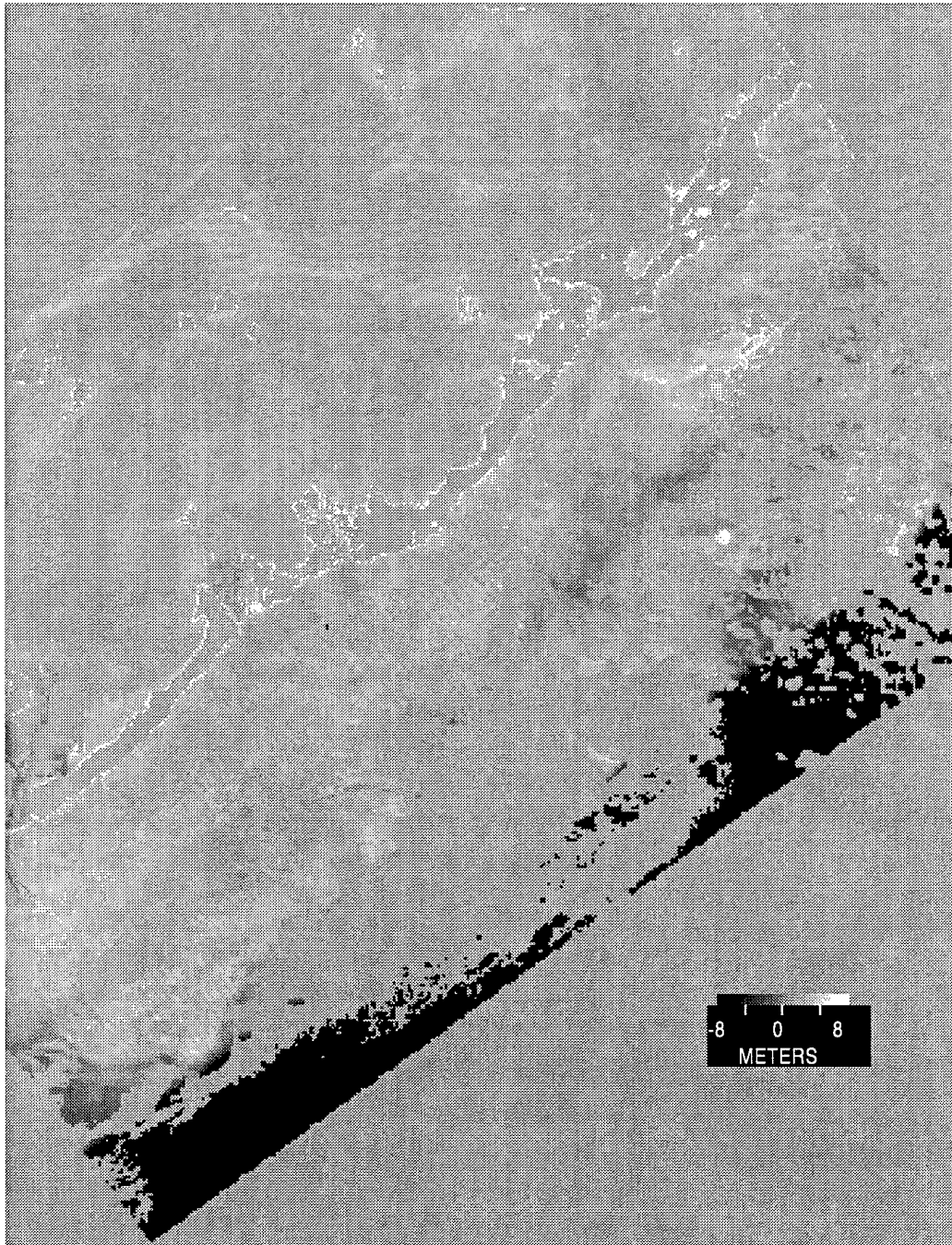

Fig. 18 – Keys depth error image. Darker shades indicate areas where the neural network estimate is too shallow, lighter shades indicate areas where the neural network estimate is too deep
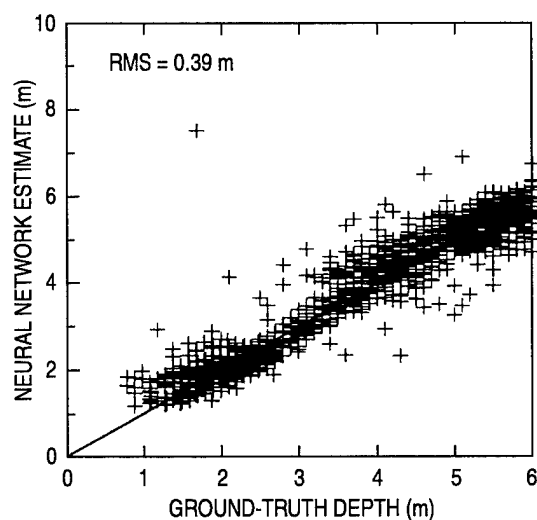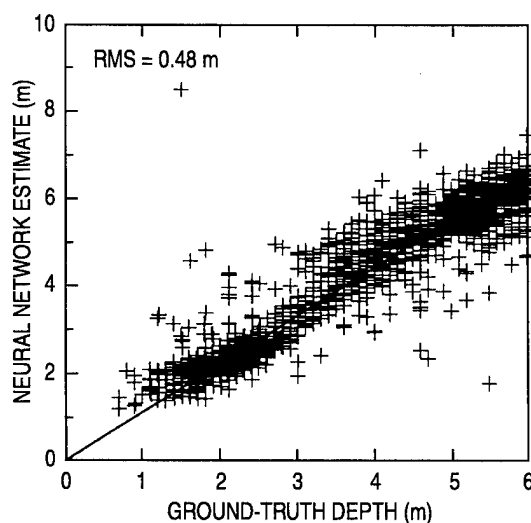
Fig. 19 – Neural network estimated depths vs.
ground-truth values for the combined test set

depth retrievals may have been possible in the Keys. The importance of good SNR performance for a hyperspectral imager used in this application is illustrated by this result. The bottom-reflected energy reaching the airborne sensor is very small, especially at the deep end of the bathymetric range of interest. High SNR is essential to extract useful information from the very weak bottom signal.

It should be noted that the relationships of spectral radiance to water depth developed here by neurocomputing methods take radiance observed at aircraft altitude as input. The steps of converting radiance to reflectance or of removing effects of atmospheric attenuation and backscatter were not required to produce these results. The effects of ocean surface transmittance of upwelling light from below and the surface reflectance of "skylight" incident from above were still present in the input. This fact is particularly significant since the correction of apparent radiance at altitude to upwelling radiance just below the sea surface is a difficult problem. It would certainly be preferable to use corrected data in the future when it is available. However, our results indicate that it is possible to produce useful bathymetry retrievals now, letting the neural network deal with the atmospheric correction and surface effects problem implicitly in the training procedure.

The difference between the ground-truth and remotely sensed depths for Tampa Bay and the Keys sites, shown in Figs. 15 and 18, respectively, show the geographical distribution of errors for each case. In the error image, white areas indicate hyperspectrally derived values deeper than ground truth; black areas indicate hyperspectrally derived values that are shallow relative to the ground truth. Mid-range gray values (the shade of the land masses) in the error image indicate areas of high accuracy. The largest errors in Tampa Bay occur in the shipping channel and other deep areas (Fig. 15). The reason for this is that the bottom is visible to the hyperspectral sensor only down to approximately 6 m. Beyond that depth, all pixels look the same regardless of depth. Therefore, in the ship channel where depths range from 12 to 25 m, and other areas where the water depth exceeds 6 m, the neural network naturally underestimates the depth. This is not really an error, but just a limitation on optical remote sensing of water depth. Another area of large errors is in the Bunces Pass north of Mullet Key (upper right edge of Fig. 15). This channel is reported as approximately 6 m deep on the NOAA (National Oceanic and Atmospheric Administration) chart, but the neural network does not estimate any depths greater than 3.5 m in this channel. The reason for this discrepancy is not known. It is possible that the water properties or bottom reflectances

in that channel differ significantly from those found in the rest of the scene. Bunces Pass covers such a small area and contains so few ground-truth points that a different bottom/water type may not be adequately represented in the training set.

The error image for the Keys (Fig. 18) shows large errors in the deep, offshore areas. The explanation for this result is the same as for the deep areas of Tampa Bay. The remainder of the Keys error image shows mostly midrange gray values indicating accurate depth retrievals overall with some slightly lighter and darker areas. This result is, of course, reflected in the much smaller test set of RMS errors for this site.

The work reported here shows that the neural network approach can be used as an interpolator to produce contiguous fields of depth values from a hyperspectral image where the depths are known at a large number of pixel locations that serve to train the network. The question of greater interest is whether the approach can be extended beyond interpolation to produce universal algorithms producing useful depth retrievals where extensive ground truth is not available. The hyperspectral bathymetry algorithms resulting from individual and combined training in this study produced essentially equivalent accuracy statistics. This result provides support for the fact that the neural network approach has resulted in at least some degree of universality, or in common neural network terminology, the network can generalize. The preliminary indication is that hyperspectral bathymetry algorithms can be developed that do not need to be tuned with extensive ground truth at each new experiment site. It could be argued that if the training set included representatives of numerous types of water and bottoms, the neural network training procedure would lock onto whatever is consistent throughout the training set, which would be some implicit embodiment of the physics of radiative transfer in the ocean/atmosphere system. Therefore, the neural network weight would be expected to have universal applicability to some degree. This argument has not been confirmed by experiment, but our combined training results are a first step in that direction. More hyperspectral image collections in other coastal regions coincident with quality bathymetric surveys will be required to further investigate this question.

BAND SELECTION REVISITED

The neural network study above employed 41 spectral bands to perform a depth retrieval. The previously reported PCA data indicates that the data set is probably only three-dimensional. Reduced dimensionality results from neighboring spectral channels being highly correlated, indicating that they carry essentially the same information and are, therefore, not independent observations. We now address the question of what wavelengths should be chosen for a reduced dimensionality data set.

Figure 7 showed that radiances at wavelengths in the range of 606.5 to 646.2 nm are the most highly correlated with depth. If one desired a single-channel bathymetry algorithm, a channel in this range would be the logical choice. We have selected the band centered at 606.5 nm for our single-channel algorithm based on the physical model of Eq. (23). The same channel was used to train a neural network with a single input to produce a bathymetry algorithm. The single-channel neural network algorithm resulted in RMS depth errors of 0.83 m compared with 1.44 m for the retrieval based on Eq. (23). The inputs to these algorithms were identical, yet the neural network result was far superior to the result based on the simple radiative transfer model. The reason for the difference is that many assumptions and simplifications were required to derive the single-channel equation. The neural network, on the other hand, was trained on the observational data as it existed without the requirement of any a priori assumptions.

Now, if a two-channel algorithm was desired, what second wavelength would be the best choice to add to 606.5 nm? To select a second wavelength, the errors in the single-channel neural network retrievals were correlated with the 40 unused channels. The unused channel most strongly correlated with the errors was the channel at 1202.0 nm. Therefore, the 1020.0-nm channel was added to the 606.5-nm channel as input to train a two-channel neural network algorithm. Note that this second channel selected is one of the channels added for atmospheric correction purposes. The RMS error for the two-channel algorithm was 0.71 m compared to 0.83 m for the single-channel case. To select a third channel, the 39 unused channel radiances were correlated with the errors from the two-channel algorithm and the channel most highly correlated with the error was selected as the third channel, in this case, the channel centered at 399.9 nm. The three-channel neural network algorithm resulted in an RMS error in the depth estimates of 0.59 m. Selection of fourth, fifth, and subsequent channels for inclusion in the neural network training proceeded in the same manner. That is, unused channels were correlated with the errors of the n-channel algorithm with the most highly correlated channel being added as the additional input for the $(n + 1)$ channel algorithm. Table 2 summarizes the results of this channel selection procedure.

Note in Table 2 that when 10 channels are included in the algorithm the error is 0.50 m, which is nearly as small as the 0.48-m value resulting when all 41 channels are used. This result is in general agreement with our PCA-based conclusion that the data set was essentially three-dimensional. Two different methods, PCA and the add-one-correlated-channel-at-a-time method, have led to the same general conclusion that approximately three to seven spectral bands are all that are required to perform bathymetry retrievals. Does this result indicate that hyperspectral data (several tens of bands) is unnecessary? The answer to that is not available. The counter argument to the results presented here is that although only three to seven channels may be required for a given set of water/bottom types, the wavelength selection will be different when the water/bottom type changes. Therefore, hyperspectral data must be collected to ensure that the correct wavelengths for the reduced band set will be available. The validity of the counter argument can only be demonstrated by collecting hyperspectral imagery and depth ground-truth data for diverse geographic locations containing a wide variety of water and bottom types to see if optimal band selection does indeed change drastically from site to site.

Table 2 – Channel Selection and Resulting Depth Errors for Neural Network Algorithms

Ch 1	Ch 2	Ch 3	Ch 4	Ch 5	Ch 6	Ch 7	Ch 8	Ch 9	Ch 10	Error (m)
606.5	-	-	-	-	-	-	-	-	-	0.83
606.5	1202	-	-	-	-	-	-	-	-	0.71
606.5	1202	399.9	-	-	-	-	-	-	-	0.59
606.5	1202	399.9	741.8	-	-	-	-	-	-	0.58
606.5	1202	399.9	741.8	866.1	-	-	-	-	-	0.57
606.5	1202	399.9	741.8	866.1	1020	-	-	-	-	0.58
606.5	1202	399.9	741.8	866.1	1020	732.2	-	-	-	0.58
606.5	1202	399.9	741.8	866.1	1020	732.2	586.6	-	-	0.52
606.5	1202	399.9	741.8	866.1	1020	732.2	586.6	576.6	-	0.50
606.5	1202	399.9	741.8	866.1	1020	732.2	586.6	576.6	556.8	0.50
All 41										0.48

SENSITIVITY ANALYSIS

What sensitivity of the hyperspectral sensor is required for the bathymetry retrieval application? It has been argued, for example, that the sensitivity of the Hyperspectral Imager on the NASA Lewis Spacecraft was not adequate for most ocean applications including bathymetry. The neural network defined quantitative relationships developed here between spectral radiance and depth can be utilized to formulate a preliminary answer to the question of sensitivity. The individual inputs to the trained neural network can be adjusted slightly and the resulting change in the estimated depth observed. The change in the depth estimate (Δd) resulting from the small change in the input radiance (ΔL) gives the sensitivity of retrieval to the input values, $\Delta d/\Delta L$. Knowing the sensitivity of the depth retrieval to changes in radiance and being able to measure the noise equivalent radiance, $NE\Delta L$, of the sensor by calculating variance in a box of pixels over uniform, offshore water, the noise equivalent depth change, $NE\Delta d$, can be calculated

$$NE\Delta d = NE\Delta L \left(\frac{\Delta d}{\Delta L} \right). \tag{24}$$

Equation (24) could be applied at each wavelength to define $NE\Delta d$ as a function of wavelength. However, for this report, only the wavelength of maximum correlation of radiance with depth (606.5 nm) is considered. The single-channel neural network algorithm that was generated to produce the values in the first row of Table 2 was used for this purpose. The input to the network was altered and the resulting change in the depth output was observed leading to a sensitivity value of 310 digital counts/m. The variance in a 10 × 10 pixel box over uniform, deep water was measured to be 15.7 digital counts for the Tampa Bay image and 18.8 digital count for the Keys image. Based on these numbers, the $NE\Delta d$ for these data sets is approximately 0.055 m, which is certainly low enough to meet Navy needs. The fact that the deep-water variance was approximately the same for the Keys and Tampa images is a surprise in view of the improvements in AVIRIS SNR, which were claimed to have occurred between the two acquisitions (see following section).

SPECTRAL RESOLUTION

Narrow spectral bands lead to lower SNR since fewer photons are available in a channel as the spectral range of acceptance of the channel is decreased. The dimensionality analysis has shown that only three to seven spectral bands are required. These facts combine to raise the following question. Since only a small number of channels are required, should this reduced band set be spectrally broader to improve SNR? This is a tradeoff situation. Broader bands lead to loss of spectral resolution, but a gain of SNR. Which factor will dominate in this case? Will the loss of bathymetry information resulting from worse spectral resolution exceed the gains available from improved SNR? As a first look at this tradeoff, the seven-channel (399.9, 606.5, 732.2, 741.8, 866.1, 1019.6, and 1202.0) neural network algorithm was trained for the combined Tampa Bay and Keys data that produced depth estimates with an RMS error of 0.58 m. Each of the seven channels was then broadened by averaging its radiance value with the radiances of its neighbors. The number of inputs to the neural network remained at seven, but the spectral resolution was now 30 nm rather than 10 nm. The neural network algorithm resulted in RMS errors of 0.59 m. A second broadening step was taken by averaging the seven channels with two neighboring channels on each side, producing an effective 50-nm resolution. The neural network operating on these seven 50-nm channels resulted in an RMS error of 0.61 m. In broadening the spectral bands from

10 to 30 nm, the RMS error increased by 2% and by 5.3% when the resolution was lowered to 50 nm. The loss of spectral resolution seems to have a slightly larger adverse effect than the benefit from improved SNR. However, the change is not dramatic, indicating that these opposing effects are nearly balanced and that no significant gain should be expected to result from averaging bands to improve SNR. Note that these results apply only to AVIRIS, which already has a very high SNR. For other hyperspectral systems with low SNR, a worthwhile gain might result from broadening the spectral response of the channels. Improved SNR can also be gained by spatial averaging. This tradeoff was not examined in this study.

DISCUSSION AND CONCLUSIONS

The depth retrievals from the Keys site are significantly more accurate than those from Tampa Bay. The larger errors for Tampa Bay can be attributed to two major causes. The first is the large time separation between the ground truth and the airborne data collections. Depths may have changed significantly between the ground and the airborne collections resulting in an unknown, but significant, portion of the Tampa Bay errors. The second factor is the SNR of the AVIRIS instrument, which has constantly improved during the AVIRIS lifetime. The SNR for the AVIRIS reference radiance at 608 nm (the approximate wavelength of maximum correlation of radiance to depth) was 923 during the 1996 collection in the Keys, but was only 535 in 1993 during the Tampa Bay experiment (Green 1998; Green et al. 1995). Hence, more accurate depth retrievals may have been possible in the Keys. The improvement in SNR reported by NASA did not seem to be borne out by the present data set, so we hesitate to invoke this explanation for improved performance in the Keys. At this time, the factors leading to improvement in the Keys data set cannot be identified.

It should be noted that the relationships of spectral radiance to water depth developed here by neurocomputing methods take radiance observed at aircraft altitude as input. The steps of converting radiance to reflectance, or of removing effects of atmospheric attenuation and backscatter were not required to produce these results. The effects of ocean surface transmittance of upwelling light from below and the surface reflectance of ìskylightî incident from above were also still present in the input. This fact is particularly significant since the correction of apparent radiance at altitude to upwelling radiance just below the sea surface is a difficult problem. It would certainly be preferable to use corrected data in the future when it is available. However, our results indicate that it is possible to produce useful bathymetry retrievals now, letting the neural network deal with the atmospheric correction and surface effects problem implicitly in the training procedure.

The difference between the ground truth and remotely sensed depths for Tampa Bay and the Keys sites (shown in Figs. 9 and 12, respectively) shows the geographical distribution of errors for each case. In the error image, white areas indicate hyperspectrally derived values deeper than ground truth and black areas indicate hyperspectrally derived values that are shallow relative to the ground truth. Mid-range gray values (the shade of the land masses) in the error image indicate areas of high accuracy. The largest errors in Tampa Bay occur in the shipping channel and other deep areas (Figure 9). The reason for this is that the bottom is visible to the hyperspectral sensor only down to approximately 6 m. Beyond that depth, all pixels look the same regardless of depth. Therefore, in the ship channel where depths range from 12 to 25 m and other areas where the water depth exceeds 6 m, the neural network naturally underestimates the depth. This is not really an error, but just a limitation on optical remote sensing of water depth. Another area of large errors is in the Bunces Pass north of Mullet Key (upper right edge of Fig. 9). This channel is reported as approximately 6 m deep on the NOAA chart, but the neural network does not estimate any

depths greater than 3.5 m in this channel. The reason for this discrepancy is not known. It is possible that the water properties or bottom reflectances in that channel differ significantly from those found in the rest of the scene. Bunces Pass covers such a small area and contains so few ground-truth points that a different bottom/water type may not be adequately represented in the training set.

The error image for the Keys (Fig. 12) shows large errors in the deep, offshore areas. The explanation for this result is the same as for the deep areas of Tampa Bay. The remainder of the Keys error image shows mostly midrange gray values indicating accurate depth retrievals overall with some slightly lighter and darker areas. This result is, of course, reflected in the much smaller test set RMS errors for this site.

The work reported here shows that the neural network approach can be used as an interpolator to produce contiguous fields of depth values from a hyperspectral image where the depths are known at a large number of pixel locations that serve to train the network. The question of greater interest is whether the approach can be extended beyond interpolation to produce universal algorithms producing useful depth retrievals where extensive ground truth is not available. The hyperspectral bathymetry algorithms resulting from individual and combined training in this study produced essentially equivalent accuracy statistics. This result provides support for the fact that the neural network approach has resulted in at least some degree of universality, or in common neural network terminology, the network can generalize. The preliminary indication is that hyperspectral bathymetry algorithms can be developed that do not need to be tuned with extensive ground truth at each new experiment site. It could be argued that if the training set included representatives of numerous types of water and bottoms, the neural network training procedure would lock on to whatever is consistent throughout the training set, which would be some implicit embodiment of the physics of radiative transfer in the ocean/atmosphere system. Therefore, the neural network weight would be expected to have universal applicability to some degree. This argument has not been confirmed by experiment, but our combined training results are a first step in that direction. More hyperspectral image collections in other coastal regions coincident with quality bathymetric surveys will be required to further investigate this question.

This study has shown a great deal of redundancy of information within the spectral bands examined. It appears that bathymetry can be retrieved from three to seven spectral bands as accurately as it can from 41 bands. It is not known whether the number of bands and spectral placement of bands found to be appropriate for this data would apply to other geographic locations.

This study has also shown that depths as large as 6 m can be retrieved from apparent spectral radiance data. This depth limit applies only to this data set. In general, lower bottom reflectance and more turbid water tend to decrease the range of depth retrievals, while higher bottom reflectance and clearer water will tend to extend the depth range.

The analysis and conclusions reported here are based on only two data sets. Furthermore, the analysis procedures have not been as detailed and thorough as they could have been if more support was available for this work. Therefore, the reader is cautioned that these conclusions are tentative, not definitive, and that further work is called for. However, we have made some significant first steps toward quantifying the possibilities and limitations of hyperspectral systems for observing water depth and have shown that the neural network approach may have merit.

ACKNOWLEDGMENTS

Hyperspectral Remote Sensing Project, Dr. Curtiss Davis, Project Manager; and the Navy Office for the Tactical Exploitation of National Capabilities (TENCAP), CDR Mike Jelinek, Program Manager. Mr. James Goudeau of the Naval Research Laboratory, Remote Sensing Applications Branch, conducted the bathymetry survey at the Florida Keys site.

REFERENCES

Apel, J. R., *Principles of Ocean Physics,* International Geophysics Series, 38, Academic Press, London, 1987.

Bierwirth, P. N., T. J. Lee, and R. V. Burne, "Shallow Sea-Floor Reflectance and Water Depth Derived by Unmixing Multispectral Imagery," *Photogrammetric Engineering and Remote Sensing* **59**, 331–338 (1993).

Carder, K. L., P. Reinersman, R. F. Chen, and F. Muller-Karger, "AVIRIS Calibration and Application in Coastal Oceanic Environments," *Remote Sens. Environ.* **44**, 205–216 (1993).

Chrien, T. G., R. O. Green, and M. L. Eastwood, "Accuracy of the Spectral and Radiometric Laboratory Calibration of the Airborne Visible/Infrared Imaging Spectrometer (AVIRIS)," Proceedings of the Second Airborne Visible/Infrared Imaging Spectrometer (AVIRIS) Workshop, Pasadena, CA, 1990.

Green, R. O., "Inflight Validation of AVIRIS Calibration in 1996 and 1997," *Summaries of the Seventh Annual JPL Airborne Earth Science Workshop,* Pasadena, CA, 1998.

Green, R. O., J. E. Conel, M. Helmlinger, J. van den Bosch, and P. Hajek, "In-Flight Radiometric Calibration of AVIRIS in 1994," *Summaries of the Fifth Annual JPL Airborne Earth Science Workshop,* Pasadena, CA, 1995.

Hamilton, M. K., C. O. Davis, W. J. Rhea, S. H. Pilorz, and K. L. Carder, "Estimating Chlorophyll Content and Bathymetry of Lake Tahoe Using AVIRIS Data," *Remote Sens.Environ.* **44**, 217–230 (1993).

Jerlov, N. G., *Marine Optics,* Elsevier Scientific, Amsterdam, 1976.

Johnson, R. A. and D. W. Wichern, "Applied Multivariate Statistical Analysis," Prentice-Hall, Inc., Englewood Cliffs, NJ, pp. 361–400, 1982.

Jupp, D. L., "Background and Extensions to Depth of Penetration (DOP) Mapping in Shallow Coastal Waters," *Symposium on Remote Sensing of the Coastal Zone,* Gold Coast, Queensland, Session 4, Paper 2, 1988.

Khan, M. A., Y. H. Fadlallah, and K. G. Al-Hinai, "Thematic Mapping of Subtidal Coastal Habitats in the Western Arabian Gulf Using Landsat TM data – Abu Ali Bay, Saudi Arabia," *Int. J. Remote Sensing* **13**, 605–614 (1992).

Lippman, R. P., "An Introduction to Computing with Neural Nets," *IEEE ASSP Magazine* **4**, 4–22 (1987).

Lyzenga, D. R., "Shallow-Water Bathymetry Using Combined Lidar and Passive Multispectral Scanner Data," *Int. J. Remote Sensing* **6**, 115–125 (1985).

Mobley, C. D., *Light and Water; Radiative Transfer in Natural Waters,* Academic Press, San Diego, CA, 1994.

Nordman, M. E., L. Wood, J. I. Michalek, and J. L. Christy, "Water Depth Extraction from Landsat-5 Imagery," Proceedings of the Twenty-Third International Symposium on Remote Sensing of Environment, pp. 1129–1139, 1990.

Paredes, J. M. and R. E. Spero, "Water Depth Mapping from Passive Remote Sensing Data Under a Generalized Ratio Assumption," *Applied Optics* **22**, 1134–1135 (1983).

Polcyn, F. C. and I. J. Sattinger, "Water Depth Determination Using Remote Sensing Techniques," Proceedings of the Sixth International Symposium on Remote Sensing of Environment, Ann Arbor, MI, 13–16 Oct 1969, pp. 1017–1028.

Walker, C. and M. Kalcic, "Gram-Schmidt Orthogonalization Technique for Atmospheric and Sunglint Correction of Landsat Imagery," *SPIE Proceedings Series* **2315**, 799–812 (1994).

Vane, G., R. O. Green, T. G. Chrien, H. T. Enmark, E. G. Hansen, and W. M. Porter, "The Airborne Visible/Infrared Imaging Spectrometer (AVIRIS)," *Remote Sens. Environ.* **44**, 127–143 (1993).

Vane, G. and A. F. H. Goetz, "Terrestrial Imaging Spectrometry: Current Status, Future Trends," *Remote Sens. Environ.* **44**, 117–126 (1993).